ETH-Bibliothek Zürich, E-Periodica, https://www.e-periodica.ch

Fluid Inclusions Studies in Quartz from Fissures of Western and Central Alps

By *Bernard P. Poty* (Nancy)*), *Hans A. Stalder* (Bern)**) and
Alain M. Weisbrod (Nancy)*)

With 12 figures and 8 tables in the text and 1 plate

Abstract

Fluid inclusions in quartz crystals of more than 120 alpine fissures from western and central Alps (Pelvoux, Mont Blanc, Aar, Gotthard and the Pennines) have been studied.

Microthermometry (freezing and heating) gives estimates of the chemical composition of the fluids in terms of three components: water, NaCl (for all the salts) and CO_2. Density estimates may be inferred as well. It is shown that fluids are mainly salt aqueous solutions, excepted in the Gotthard and the Pennines, where CO_2 becomes an important component.

Chemical analyses of fluids occuring in inclusions give the relative amounts of the following solute components: K, Na, Ca, Mg and to a lesser extent, Cl and SO_4. The K/Na ratio seems to be well buffered in feldspars-bearing rocks. After it has been shown that albite grew in the disordered structural state, even at rather low temperatures, the equilibrium constants of the system adularia- high albite-KCl-NaCl aqueous solution are calculated and used as a tentative geothermometer. Pressures and depths of formation have been estimated using the calculated (from microthermometry results) densities of the fluids.

Estimated temperatures increase from the Pelvoux massif (340° C) to the Gotthard massif (505° C). On the other hand the pressure (2.5 to 3 Kbar) and the overburden (9.5 to 11 km) are rather constant all over the Mont Blanc and Aar massives.

Zusammenfassung

Flüssigkeits- und Gaseinschlüsse von Quarzkristallen aus mehr als 120 alpinen Zerrklüften der West- und Zentralalpen (Pelvoux-, Mont Blanc-, Aar- und Gotthard-Massiv, Penninikum) sind untersucht worden.

Mikrothermometrische Messungen der flüssigen und gasförmigen Einschlussfüllungen auf dem Kühl- und Heiztisch führen zu Abschätzungen der drei Komponenten H_2O,

Authors' adresses:

*) Equipe de Recherche sur les Equilibres entre Fluides et Minéraux, C.R.P.G.,C.O. n° 1 – 54500 – Vandœuvre-les-Nancy and E.N.S.G., B.P. 452 – 54000 – Nancy (France).

**) Naturhistorisches Museum Bern, Bernastrasse 15, 3005 Bern (Switzerland).

NaCl (als Mass für alle Salzanteile) und CO_2, und ebenso zur Abschätzung der Dichten der fluiden Phasen. Es wird gezeigt, dass die Einschlussfüllungen vorwiegend aus Salz-lösungen bestehen; einzig im Gotthardmassiv und im Penninikum ist zudem CO_2 eine wichtige Komponente.

Chemische Analysen der fluiden Phasen in den Einschlüssen geben die Relativgrössen der Kationen K, Na, Ca und Mg. Auch die Relativgrössen der Anionen Cl und SO4 wur-den zum Teil bestimmt.

Das K/Na-Verhältnis scheint in feldspatführenden Gesteinen gut gepuffert zu sein. Es wird gezeigt, dass der Albit (der alpinen Zerrklüfte) in der ungeordneten Struktur-varietät auskristallisiert ist, auch bei relativ tiefen Temperaturen. Deshalb kann versucht werden, die Gleichgewichtskonstanten des Systems Adular-Hochalbit/KCl-NaCl der wässerigen Lösung als geologisches Thermometer zu gebrauchen. Der Bildungsdruck und die Gesteinsüberlagerung werden ebenfalls abgeschätzt, dies auf Grund der Bildungs-temperatur und der Dichte der Einschlussfüllungen (letztere als Ergebnis der Mikro-thermometrie).

Die abgeschätzten Temperaturen nehmen vom Pelvoux-Massiv (340° C) zum Gott-hard-Massiv (505° C) zu. Auf der andern Seite sind der bestimmte Druck (2,5 bis 3,0 Kbar) und die Gesteinsüberlagerung (9,5 bis 11 km) für das Mont-Blanc- und das Aar-Massiv mehr oder weniger konstant.

INTRODUCTION

Alpine fissure minerals from Switzerland have been described by KENNGOTT (1866), KOENIGSBERGER (1919, 1940), P. NIGGLI (1940), PARKER (1940, 1953) and STALDER, DE QUERVAIN, E. NIGGLI and GRAESER (1973, revised edition of PARKER, 1953). Most alpine fissure minerals from the French alps have been described by LACROIX (1893–1913). In the Soviet union, where fissure minerals occur commonly in the Urals and the Caucasus a considerable amount of work has also been done. GRIGORIEV (1960) gives a review of these works.

The relations between fissure mineral formation and alpine metamorphism are still being discussed. Radiometric dating isotopic measurements and fluid inclusion studies should help to gain an understanding of these relationships.

Radiometric dating (Rb/Sr and K/Ar) have been performed on several fissure minerals (JÄGER et al. 1967, LEUTWEIN et al. 1970, ARNOLD 1972, PURDY and STALDER 1973). Some of the published data are listed in table I. Radiometric dating can only indicate the time when minerals ceased being in interaction with fissure solutions. In the Mont-Blanc massif ages for fissure minerals (adularia and muscovite) are quite distinct from those of country rock minerals. Ages of fissure minerals might be true ages. In the Aar massif some K/Ar values are useless because of demonstrated argon over-pressures during growth. In the Simplon area the K/Ar method gives a consistent dif-ference of 4 my between country rock and fissure minerals. But in many places country rock and fissure mineral give the same cooling age.

The presence of fluid inclusions in alpine fissure minerals has been known for a long time but attention has been focused on them only in the last decade.

Table I. *Selected Ages of Alpine Fissure Minerals*

Locality	Method	Mineral (f) fissure (r) rockforming	Age in million years (different rocks or minerals)	Literature
Mt-Blanc-Massif				
Fissure Nr. 64–207	Rb-Sr	Mu (f)	14,8	LEUTWEIN et al. (1970)
	K-Ar	Mu (f)	13,5 ± 2; 13,4 ± 2	LEUTWEIN et al. (1970)
Fissure Nr. 68–001	K-Ar	Ad (f)	18,3 ± 2; 15,8 ± 2	LEUTWEIN et al. (1970)
Gotthard-Massif				
Freilaufstollen Val Casatscha-	K-Ar	Mu (f)	16,0 ± 0,5	PURDY, STALDER (1973)
Sta Maria	Rb-Sr	Bi (f)	16,3 ± 0,8; 16,7 ± 0,9; 16,7 ± 0,7 16,0 ± 0,9	ARNOLD (1972)
	Rb-Sr	Bi (r)	16,8 ± 1,7; 17,9 ± 2,0; 16,6 ± 2,0	ARNOLD (1972)
Pennines				
Simplontunnel different fissures	K-Ar	Mu (f)	9,8 ± 0,3; 10,2 ± 0,4	PURDY, STALDER (1973)
	K-Ar	Ad (f)	8,5 ± 0,1; 8,2 ± 0,1	PURDY, STALDER (1973)
	K-Ar	Mu (r)	14	PURDY, JÄGER (in prep.)
	Rb-Sr	Bi (f)*)	14,3 ± 2,7; 12,8 ± 0,9; 12,7 ± 2,4 12,0 ± 2,3	JÄGER et al. (1967)
	Rb-Sr	Bi (r)	11,0 ± 1,0	JÄGER et al. (1967)
Cavagnöö, Val Bavona	K-Ar	Mu (f)	13,7 ± 0,4	PURDY, STALDER (1973)
	K-Ar	Ad (f)	13,6 ± 0,2	PURDY, STALDER (1973)

*) Fissure biotites but not from open fissures.

As early as 1906 KOENIGSBERGER and MÜLLER gave two chemical analyses performed on big inclusions from the Aar massif. Those two analyses were probably the first ever made on a metamorphic fluid. DEICHA (1949, 1955) began a series of studies performed with a variety of methods. Thermometry under the microscope (microthermometry), was the main method used by YPMA (1963) on Belledonne, STALDER (1963) on the Grimsel (Aar), POTY (1967–1969) on quartz from La Gardette (type locality of Dauphiné habit) and Mont-Blanc, STALDER and TOURAY (1970), MULLIS et al. (1973) on quartz from the northern calcareous alps. Besides those essentially microthermometric studies TOURAY (1968) gave mass spectrometric analyses of gases.

All these studies gave a picture of fluids associated with a phase of alpine metamorphism. This paper continues in broadening the region of sampling (Pelvoux, Mont-Blanc, Aar, Gotthard and the Pennines), with increasing the number of samples, and with improving the accuracy of microthermometry data. Chemical analyses of leachates are given and a new method determining temperature is proposed leading to T-P estimates of alpine fissures formation.

I. Data from Microthermometry

Analytical techniques

Generally speaking, microthermometry consists of measuring, under the microscope, the temperatures of physical changes undergone by the fluid phases trapped in inclusions.

Investigations were performed at Nancy and Fribourg with the aid of identical heating and freezing stages, designed to work in the -160 to $+380°$ C range. These apparatus were built in the CRPG at Nancy.

The lower temperatures are obtained by nitrogen gas previously cooled in liquid nitrogen and flowing through the stage. After inclusions have been frozen, they are slowly warmed at a constant rate of 1 to $2°$ C/minute, by controlling the gas flow with a precision-valve. High temperatures are obtained with a heating resistance.

Temperatures are measured with a platinum resistance sensor set very close to the sample. Measurements are standardized against the melting points of various high purity chemicals, such as hexane ($-94.3°$ C), heptane ($-90.6°$ C), n-dodecane ($-9.6°$ C) and distilled water ($0.0°$ C). Natural CO_2-inclusions from Calanda (checked for purity by TOURAY, 1968; melting point: $-56.6°$ C) were also used. Standardization at high temperatures was made with special chemicals from Merck Corporation.

The precision of measurements is about $\pm 0.2°$ C in the range -12 to $+31°$ C, and $\pm 1.5°$ C in the range -150 to $+350°$ C.

The procedure of investigation has been described in detail by ROEDDER (1962). For two phase inclusions, the following temperatures were measured: lower melting point (solidus or eutectic temperature), higher melting point (liquidus, often called "freezing point" in this paper), dissociation of possible hydrates, homogenization. Possible occurrence of CO_2 was checked with a crushing stage (DEICHA, 1955; ROEDDER, 1970). For inclusions with liquid CO_2, the temperature of melting of frozen CO_2 and the temperature of homogenization of the two CO_2-rich phases were also determined. Quite often, inclusions with an immiscible CO_2-rich phase decrepitated before reaching the temperature of bulk-homogenization of the fluid.

Although various components are present as solute species, aqueous solution is usually described in terms of the theoretical $NaCl$-H_2O system. Thus, it is possible to calculate an "NaCl equivalent" content from the liquidus temperature.

The determination of salt content in the CO_2-rich inclusions is difficult, because of the formation of CO_2-hydrate (CO_2-5.7 H_2O). Less CO_2-hydrate crystallizes when a fast cooling rate is used than with a slow cooling rate ($1°$ C/min.). In the latter case, salt concentration increases considerably because more water is used during hydrate formation. In other studies, differences up to $1°$ C in the freezing point of the aqueous solutions, due to variable cooling rates, were observed. The data given in this paper are for the rapid cooling rate of $20°$ C/min.

RESULTS

Many quartz samples and a few axinites (Pelvoux) from more than 120 fissures were investigated. Most inclusions appear in healed fractures (secondary inclusions), but some primary inclusions were also recognized.

The most important results are listed in table II and III, and need some general comments.

Table II. *Examples of variations of salt and CO_2 content in fluid inclusions*

Belvedere, Furka (Q 113) and *Grasso di Froda I* (kr 24)

Nr. of the inclusion	Melting temp. aqueous solution	Melting temp. CO_2-hydrate	Equival. [NaCl] weight %	Homogen. temperature
Q 113–1	–0,9	–	1,5	194
Q 113–2	–2,0	–	3,4	207
Q 113–3	–2,1	–	3,6	208
kr 24–1	–2,75	9,9	4,6	245
kr 24–2	–2,9	9,6	4,8	272
kr 24–4	–3,0	9,1	5,0	274

Fluh, St. Niklaus (6713)

Nr. of the inclusion	Homogen. of the liquid and the gas. CO_2-phases	Vol. percent of the CO_2-phase	Density of the CO_2-phase at the homog. temp.	Remarks
6713/1, 2	29 L	90	0,63	Salt content of the H_2O-rich phase ± constant at 5,5% [NaCl] eq.
6713/3–5	24 G	85	0,22	
6713/8	20 G	45	0,19	

1. Although age relationships between secondary inclusions are difficult to detect, it seems that the older inclusions are more concentrated in salt. Examples of average values are given in table II. The largest variations are observed in the neighbourhood of evaporitic sediments (e.g. = Camperio, Bitsch, Lengenbach).

2. Some older fluids are CO_2-rich. In such inclusions, a strong decrease of the CO_2 content from the inner to the outer part of the quartz crystals is usually observed (see table II). On the other hand, late CO_2-rich fluids are well known all over the Alps, mainly in the so-called sceptre-quartz; they are not considered in this paper.

3. Besides CO_2, other trace gases are present in the inclusions, as shown by mass-spectromeric analyses (TOURAY, 1968; ZIMMERMANN and POTY, 1970). Although quantitative estimations are not possible with microthermometry, such gases have been detected here. At Kammegg, for instance, an unknown hydrate was discovered and probably indicates the presence of hydrocarbon.

However, the melting temperature of CO_2-rich phase in the inclusions investigated here departs only slightly from the melting temperature of pure $CO_2(-56.6°$ C). Out of 40 determinations, 33 are between -56 and $-57°$ C, and the others remain very close to these values. Therefore, the vapor phase of three-phase inclusions from alpine quartz contains almost pure CO_2.

4. The dissociation temperatures of the CO_2 hydrate that have been measured here are scattered in the range $+7$ to $+11.5°$ C. According to LARSEN (1956), these variations can be related mainly to the salt content of the aqueous solution (a high salt content decreases the dissociation temperature).

5. Some data about the solidus temperature of the aqueous solutions have already been given and discussed (POTY and STALDER, 1970). The new data

confirm the former conclusions, and we have abstained from any discussion here.

6. Although the calculated compositions of the inclusions are based upon estimates and involve some simplifications, they give more reliable values than many of the mass-spectrometric analyses, for the later often give only average composition of different generations of inclusions. Moreover, the interpretation of mass-spectrometric analyses is made difficult by problems such as irreversible adsorption of some gases on surfaces.

<div align="center">Table III. Microthermometry results</div>

<div align="center">H_2O-rich phase (1)–(3)</div>

(1) Liquidus temperature ("freezing point") in $°C$.

(2) Concentration of NaCl (wt %) of the theoretical $NaCl$-H_2O aqueous solution, the freezing point of which is the same as the freezing point of the real solution, given in column (1). Liquidus curve from Scatchard and Prentiss (1933) and Rodebush (1918).

(3) Density of the aqueous solution refered to the $NaCl$-H_2O system.

<div align="center">CO_2-rich phase (4)–(6)</div>

(4) Homogenization temperature of the two CO_2-rich phases, in three phase inclusions (G = homogenization in vapor state, L = homogenization in liquid state). In two phase inclusions, the CO_2 content is estimated from runs with the crushing stage, and indicated as follows:

　　　0: no CO_2 detectable,
　　　x: traces of CO_2 (about 1,5 wt %),
　　xx: some CO_2 (about 3 wt %),
　xxx: some more CO_2 (about 4,5 wt %).

(5) Volume percent of the CO_2-rich phase from a microscopic estimation.

(6) Density of the CO_2 phase at the homogenization temperature from the P-V-T data after different authors in Landolt-Börnstein (1960).

(7) Bulk homogenization temperature of the fluid phases in $°C$. The number of fluid phases at room temperature is given in brackets. The values refer to the representative interval or representative highest value.

(8) to (10) Estimated composition of the fluid phase, in terms of the components $NaCl$-H_2O-CO_2.

(8) H_2O in weight percent.

(9) Equivalent [NaCl] in weight percent.

(10) CO_2 in weight percent; calculated from volume percentage (estimated under the microscope) and from the density of homogenized CO_2. The content of CO_2 in the aqueous solution coexisting with liquid CO_2 was taken to be 5.5 wt % at 25° C and 63 bars (Wiebe and Gaddy, 1940). This mean value is too high for salt-rich inclusions, too low for pure water.

(11) Number of studied inclusions.

(12) Notes, remarks:
　　　(7) = (1)　Homogenization and cryometry were made on the same inclusions.
　　　(7) ~ (1)　Homogenization and cryometry were made on analogous inclusions.
　　　(7) ≠ (1)　Homogenization and cryometry were made on different inclusions, homogenization generally on younger ones.
　　G: during the total homogenization the liquid phase disappears. Without remarks: the gaseous phase always disappears.

Table III. *Microthermometry results*

Locality	H_2O-rich phase (1) T_c °C	(2) NaCl	(3) g/cm³	CO_2-rich phase (4) cc/gas vol.%	(5) vol.%	(6) g/cm³	Homogen. (7) °C	Approx. compos. (8) H_2O %	(9) NaCl	(10) CO_2	Number (11)	Notes (12)
Grandes Rousses and Faisces												
Alpe d'Huez	-13/-16	17	1.13				167/192 183	81	17	2	15	
Baage des Coumfères quartz anisite	-15/-27, -31/-33			x	4		168/186 180, 199/200 195	90		2	14	
Mont Blanc												
Trient	-3.7/-4.9	7.8	1.06	x	3		139/179 170	90	8	2	7	(7)-(L)
Aiguille du Tour	-4.9/-5.4	8	1.06	x	4		180/185 182	90	8	2	6	(7)-(L)
Charlet Streston		7	1.05	x	3		187/201 195	88	7	5	7	(7)-(L)
Tour Noir		7	1.05	xxx	4		215/220 215	87	7	6	5	(7)≠(L)
Col des cristaux	-3.9/-4.5		1.06	x	4		143/213 208				15	Hydrate T_f -1.5
Face Nord des Courtes I	-4.2/-5.9	7.7	1.06	x	3		171/189 185	90	8	2	7	(7)-(L)
II	-4.4/-6.4	7.3	1.05	x	4		177/187 183	90	8	2	17	(7)-(L)
III	-5.9/-6.4	7.8	1.06	x	4		145/185 175	90	8	2	14	(7)-(L)
Grande Montets	-4.4/-5.9	9.4	1.07	x	4		162/195 182	90	8	2	14	(7)-(L)
Les Rochasses	-6.4/-6.9	13.5	1.10	x	4		189/198 196	84	14	2	6	Hydrate
Bouhard	-9/-10	13.5	1.10	x	3		205/213 208	88		3	6	
Pointe Isabelle	-5.1/-6.1	8.7	1.06	x			166/186 175					Hydrate
Aiguille Pierre Jos. I	-5.4/-6.4	9	1.06	xxx	4		171/200 200	86	9	5	6	$Hydr.T_f$ 44/46
II	-5.0/-7.0	9	1.06	x	4		202/216 210	86	9	5	7	
Aig. des P. Jorasses	-5.3/-5.7	6.7	1.05	xxx	3		166/178 173	91	7	2	9	Hydrate
Les Périades	-5.9/-6.4	9.2	1.07	x	3		154/164 160	89	9	2	7	
Les Mottets	-4.0/-7.5	8	1.06	24G	8	0.15	1177/206 196	86	8	6	8	Hydrate
Aar Massif												
In Jelzel	-1.9	3.2	1.02	x	3.5	0.02	190	95	3	2	3	(7)≠(L)
Meidgbach	-5.9	9.2	1.07	xx	5	0.05	180	88	9	3	5	(7)-(L)
Jigikumbel	-5.8	9.0	1.06	xx	4	0.05	168	88	9	3	6	(7)-(L)
Gauli	-4.1	6.7	1.05	xx	3	0.05	147	90	7	3	12	(7)-(L)
Kammegg	-2.9	4.8	1.03	x	4	0.08	182	87	6	7	6	(7)≠(L)
Mittagflub-Trift	-4.0	6.5	1.05	25G	8	0.23	295(5)	91	4	5	8	(7)≠(L)
Trift	-2.6	4.4	1.03	xx	3.5	0.05	136	87	12	1	8	(7)≠(L)
Horefalli	-7.9	11.6	1.08	x	2.5	0.02	189	87	10	3	3	(7)-(L)
Vorder Ried I	-2.9	4.8	1.03	xx	4	0.05		92	5	3	5	(7)-(L)
Vorder Ried II	-6.2	9.5	1.07	x	4	0.05	173	94	4	2	4	(7)-(L)
Griessernetal	-2.4	4.0	1.03	x	4	0.02	161	90	8	2	5	(7)-(L)
Bänntal	-5.3	8.4	1.06	x	4	0.02	161	87	10	3	3	(7)-(L)
Reistital	-5.0	5.0	1.04	xx	3	0.02	165	93	5	2	5	(7)-(L)
Algmufer Platten	-6.4	9.8	1.07	xxx	4	0.05	214	89	6	5	3	(7)-(L)
Ober Sand	-5.6	5.9	1.04	x	4	0.08	270	92	5	3	5	(7)-(L)
Alp Cavrein	-2.8	4.7	1.03	xxx	4	0.05	177	93	4	3	5	(7)≠(L)
Hinter Wasen	-4.2	4.2	1.03	31G	15	0.42	243(2)	79	5	15	3	(7)≠(L)
Kl. Lauteraarhorn	-6.5	9.9	1.07	28G	12	0.29	209(3)	84	7	9	5	(7)-(L)
Vord. Zinggenstock	-4.3	7.0	1.05	o	3	0.05	199	84	13	3	10	(7)-(L)
Juchli	-0.8	12.7	1.09	x	4	0.42		92			5	(7)-(L)
Sommerloch I	-5.3	8.4	1.06	x	4	0.05	205	92	8	-	5	(7)-(L)
Sommerloch II	-10.9	15.0	1.11	x	7	0.02	201	83	15	2	5	(7)-(L)
Unt. Kassiturm	-5.9	9.2	1.07	x	6	0.02	199	89	9	2	5	(7)-(L)
Gersiengletscher	-6.0	9.3	1.07	31G	8	0.42	174(2)	82	9	-	10	(7)-(L)
Gletschhorn	-8.0	11.8	1.08	o	3	0.05	187	88	12	-	10	(7)-(L)
Giessonen I	-6.2	9.5	1.07	xx	8	0.05	208	88	10	2	3	(7)-(L)
Giessonen II	-5.6	5.9	1.04	x	8	0.02	196	92	6	2	5	(7)-(L)
Giessonen III	-4.6	7.4	1.05	x	6	0.02	194	91	7	2	2	(7)-(L)
Fodenstock	-4.1	6.7	1.05	x	4	0.05	199	91	6	3	3	(7)-(L)
Purgsboch	-5.8	6.2	1.04	x	4	0.05		91	7	2	8	(7)≠(L)
Brig	-6.0	4.7	1.03	30L	16	0.59	270(3)	77	8	15	15	(7)≠(L)
Bel Grat	-4.1	9.3	1.07	x	5	0.05	195	90	7	3	8	(7)-(L)
Müustigevgletscher	-4.2	6.7	1.05	30L	6	0.02	188	91	7	2	4	(7)-(L)
Bärfel	-5.7	6.8	1.04	x	6	0.08	216	91	6	3	3	(7)-(L)
Trübtensee	-1.8	6.1	1.02	xxx	5	0.05	185	90	7	3	6	(7)≠(L)
Gletsch	-4.8	3.1	1.05	x	6	0.08	207	90	7	3	3	(7)-(L)
Rhonegletscher	-4.4	6.7	1.05	30G	10	0.32	245(5)	88	7	5	6	(7)-(L)
Unter Aass	-3.0	7.1	1.05	x	5	0.05	220	93	5	2	3	(7)-(L)
Belvedere	-2.1	3.6	1.03	xx	4	0.05	208	93	4	3	4	(7)-(L)
Grosstal	-4.5	7.3	1.05	xx	4	0.05	175	90	7	2	9	(7)-(L)
Giessonen IV	-5.9	9.2	1.07	x	7	0.05	199	88	10	2	5	(7)-(L)
Mörtian	-6.8	10.1	1.07	x	7	0.02	206	88	10	2	10	(7)-(L)
Russeinbrücke	-4.8	6.7	1.05	x	6	0.05	197	90	7	3	15	(7)≠(L)
Flattunnig	-4.5	7.3	1.05	30,5L	75	0.55	275(5)	34	3	63	8	(7)≠(L)
Bitsch				Inclusions with big rock salt crystals and			340					
				?anhydrite. Dissolution of the rock salt at 220°.								
Gotthard Massif												
Moosbubel	-3.2	5.3	1.04	24.5L	23	0.71	145(2)	74	4	22	3	(7)≠(L)
Lauma, Fiesch	-5.1	8.1	1.06	25L	32	0.74	295(5)	65	6	29	4	(7)-(L)
Faulhorn	-5.0	8.0	1.06	20L	45	0.77		54	5	41	5	(7)≠(L)
Muttengletscher	-4.5	7.3	1.05	29.5L	41	0.61		62	5	33	6	(7)≠(L)
Pis Prevat	-4.4	7.1	1.05	28.5L	70	0.64	208	36	5	61	6	(7)≠(L)
El della Pibbia	-5.5	5.8	1.04	29,5G	17	0.31	256(3)	84	5	11	6	
La Pibbia	-7.1	10.6	1.08	28G	17	0.28		80	10	10	6	(7)≠(L)
El d'Albimessa	-3.2	5.3	1.04	23L	70	0.74	315(5)	23	1	76	3	(7)≠(L)
Alpe di Fleud	-4.0	6.5	1.05	27.5L	20	0.77		54	4	42	4	
Grasso di Froda I	-5.0	5.0	1.04	29L	27	0.63	274(5)	72	4	24	10	
Grasso di Froda II	-5.6	5.9	1.04	25L	50	0.71		52	4	44	3	(7)≠(L)
Grasso di Froda III	-6.0	9.3	1.07	29L	50	0.63	286(5)	68	7	25	7	(7)≠(L)
Foncioni Negri	-5.8	6.2	1.04	29L	40	0.63		63	4	33	5	(7)≠(L)
Alpe Stgegia I	-3.2	5.3	1.04	xx	5	0.05	252	93	5	2	4	(7)-(L)
Alpe Stgegia II	-4.5	7.0	1.05	30L	18	0.08	268	88	7	9	5	(7)-(L)
Drusi, Piatta	-7.0	10.5	1.07	28L	15	0.66		75	9	15	8	(7)≠(L)
Pis Mies	-5.5	5.5	1.04	20L	20	0.77	288(5)	75	5	20	15	(7)≠(L)
Val Cassetscha	-5.8	9.0	1.06	30G	18	0.32	264(5)	80	8	12	6	(7)≠(L)
Pis Gervisi	-5.8	9.0	1.05	30,5G	25	0.37	252(5)	77	3	15	15	(7)≠(L)
Penninm												
Gh. del Cervaghö I	-3.6	5.9	1.04	25L	40	0.74	184(2)	60	4	36	4	(7)≠(L)
Gh. del Cervaghö II	-3.7	6.1	1.04	24L	30	0.72	294(5)	68	5	27	5	(7)≠(L)
Gh. del Cervaghö III	-3.4	6.2	1.04	23L	52	0.74		50	3	47	4	(7)≠(L)
Gh. del Cervaghö IV	-0.6	1.0	1.01	o	10	-	208	99	1	-	4	(7)≠(L)
Cavaghö, Maggia	-5.75	5.7	1.04	25L	36	0.71		64	4	32	32	(7)≠(L)
Forc. di Bregn	-5.7	6.1	1.04	24L	45	0.72		56	4	40	4	(7)≠(L)
Campo Bianco	-3.7	6.1	1.04	23L	70	0.74		33	2	65	3	
Paisano	-2.0	5.0	1.04	23L	50	0.50	220(2)	69	5	21	4	(7)-(L)
Pis Stgir	-2.7	4.5	1.03	x	6	0.02		94	4	2	5	(7)≠(L)
Aquarozes	-7.5	11.1	1.08	14,5G	15	0.16		81	11	8	6	(7)-(L)/a
Frogiasco	-5.6	5.7	1.04	xxx	3	0.08		89	6	5	12	(7)≠(L)/a
Arvigo	-5.8	6.2	1.04	30L	35	0.69	338(5)	59	12	29	5	(7)-(L)
Camperio, CO_2-rich	-8.0	11.8	1.08	30L	75	0.42	350(5)	61	4	57	8	(7)≠(L)
Camperio, NaCl-rich	-18.5	21.7	1.18	30L	40	0.32	215(2)	66	20	31	38	(7)≠(L)
Campo Blanco	-5.9	6.3	1.04	22L	60	0.75		40	4	12	8	
Simplontunnel I	-5.0	5.0	1.04	28L	45	0.66	305(5)	59	5	36	4	(7)≠(L)
Simplontunnel II	-5.0	5.0	1.04	27,5L	50	0.67	300(5)	54	5	43	3	(7)≠(L)
Simplontunnel III	-5.4	6.5	1.06	27L	60	0.68		13	1	86	6	(7)≠(L)
Simplontunnel IV	-1.9	3.2	1.02	31L	85	0.50	350(5)	24	1	65	7	(7)-(L)/a
Gibelasten	-5.8	6.2	1.04	20L	70	0.77		33	2	65	6	(7)≠(L)
Lengenbach, CO_2-rich	-2.5	4.2	1.05	xx	55	0.05	265	35	4	4	3	(7)≠(L)
Gischihorn	-3.1	5.1	1.04	26L	55	0.69	310(5)	49	5	48	9	(7)≠(L)
Harkumse	-2.0	3.4	1.02	15L	90	0.84		11	-	89	8	

Leere Seite

Blank page

Page vide

Locality	≠ analysis	K ppm	Na ppm	Ca ppm	Mg ppm	Cl ppm	SO₄ ppm	K/Na at	Ca/Na at	Mg/Ca at	$\frac{Ca + Mg}{K + Na}$ at	$\frac{SO_4}{Cl}$ at	$\frac{\Sigma\ anal\ an}{\Sigma\ anal\ cat}$ eq
Pelvoux													
La Gardette	53	1.60	13.20	.194	.032			.071	.008	.272	.010		
"	56	.325	2.25	.09	.019			.085	.230	.348	.029		
"	243	1.58	22.125	.195	.005	36.5	.33	.042	.005	.042	.005	.003	1.02
"	251	1.09	12.87	.076	.015	22.5	.21	.050	.003	.325	.004	.003	1.08
"	323	1.555	17.02	.162	.000	29.20	.14	.054	.005	–	.005	.003	1.05
Alpe d'Huez	54	2.24	12.40	.522	.105			.106	.024	.332	.029		
Col de Maronne	131	2.30	14.05	.390	.003			.096	.016	.013	.015		
Rampe des Commères	87	7.60	29.40	27.60	.073			.152	.539	.004	.470		
"	137	8.70	34.30	22.131	.060			.149	.370	.004	.323		
"	138	10.31	39.00	25.74	.060			.155	.379	.004	.329		
Mont Blanc													
Trient	116	.200	.75	.037	.006			.157	.028	.267	.005		
"	117	.700	2.73	.132	.014			.151	.028	.175	.028		
Charlet Straton	42	.34	1.26	.04	.007			.159	.018	.288	.020		
"	43	1.20	4.17	.154	.019			.169	.021	.203	.022		
"	62	3.46	16.00	2.60	.056			.127	.093	.036	.085		
"	76	.455	1.72	.079	.010			.156	.026	.209	.027		
"	130	.600	2.37	.130	.001			.149	.031	.013	.028		
"	248	2.425	10.368	1.731	.008	24.2	.05	.137	.096	.008	.085	.001	1.14
Le Tour Noir	37	1.62	6.55	.181	.041			.145	.016	.373	.019		
"	40	1.76	10.70	.222	.037			.097	.012	.275	.014		
"	41	2.17	8.03	.218	.056			.159	.016	.423	.019		
"	324	.352	1.203	.000	.005	2.40	<.01	.172			.003	.000	1.10
Col des cristaux	326	.593	2.486	.004	.005	5.16	.04	.141	.001	2.06	.002	.003	1.18
Les Courtes I	242	2.59	8.834	.308	.002	17.5	.18	.170	.020	.011	.017	.004	1.07
" II	115	.455	1.55	.037	.010			.173	.014	.446	.017		
" II	114	.810	3.0	.085	.012			.159	.016	.233	.017		
" III	112	.655	2.32	.105	.116			.166	.026	.251	.028		
" III	111	.517	1.59	.138	.013			.191	.050	.155	.048		
" III	110	.472	1.785	.105	.014			.155	.034	.220	.036		
Grands Montets	118	.517	1.945	.057	.010			.156	.017	.289	.019		
"	119	.74	2.69	.118	.015			.162	.025	.210	.026		
Les Rachasses	108	.37	1.42	.118	.013			.153	.048	.182	.049		
"	109	.45	2.78	.072	.014			.095	.015	.321	.018		
Bochard	325	3.854	18.52	5.356	.002	50.00	.05	.122	.017	.001	.148	.000	1.20
Talèfre	67	2.35	8.60	.790	.029			.161	.053	.061	.048		
Pierre Joseph	327	3.301	12.03	.298	.007	23.20	.07	.161	.014	.039	.013	.001	1.05
Les Périades	113	1.53	4.96	.210	.019			.181	.024	.149	.025		
"	331	.818	3.006	.146	.003	6.40	.01	.160	.028	.034	.025	.0006	1.14
Les Mottets	126	.61	2.02	.070	.008			.178	.020	.188	.020		
"	127	.305	1.17	.024	.004			.153	.012	.275	.013		
"	128	.39	1.47	.024	.004			.156	.009	.275	.010		
"	250	3.565	18.495	.446	.024	32.5	.20	.113	.014	.089	.013	.002	1.00
Tunnel	125	2.53	11.97	1.346	.021			.124	.065	.026	.059		
"	129	1.22	6.70	3.103	.003			.107	.266	.002	.240		
Aar													
Gauli	245	.69	3.990	.188	.011	6.8	.21	.101	.027	.096	.027	.011	.98
"	330	.212	.715	.000	.004	1.48	.05	.174	.000		.004	.012	1.16
Kammegg	79	1.63	6.05	.275	.033			.158	.026	.198	.027		
Hinter Wasen	35	5.60	23.4	.447	.036			.141	.011	.133	.011		
Kl. Lauteraarhorn	23	.315	1.10	.014	.005			.168	.007	.589	.010		
Unterer Kessiturm	144	.580	2.30	.616	.051			.148	.154	.136	.152		
Gerstengletscher	33	.305	1.06	.036	.006			.169	.019	.275	.021		
"	34	2.32	7.82	.534	.024			.174	.039	.074	.036		
"	141	.510	1.87	.040	.007			.160	.012	.288	.014		
Tiefengletscher	25	1.165	3.90	.184	.020			.176	.027	.179	.027		
"	26	1.66	4.70	.116	.016			.208	.014	.227	.014		
Göschenen I	319	1.380	5.530	.176	/	11.10	.07	.147	.018		.016	.002	1.11
Göschenen II	317	1.600	6.830	.243	/	13.88	.20	.138	.020		.017	.005	1.18
Brig	328	.337	1.758	.002	.005	3.26	.25	.112	.001	4.12	.003	.028	1.13
Bärfel	329	1.304	5.56	.296	.002	11.08	.17	.138	.031	.011	.027	.006	1.09
Gletsch	88	.235	.710	.000	.003			.195	.000		.003		
"	332	.143	.489	.004	.004	.85	.02	.174	.005	1.67	.011	.009	.96
Rhonegletscher	19	.95	3.45	.098	.016			.162	.016	.268	.018		
"	143	.590	1.76	.146	.020			.197	.048	.225	.049		
Gotthard													
Faulhorn	320	.237	1.196	/	/	2.24	.20	.117				.033	1.16
Muttengletscher	246	1.185	5.865	.459	.028	10.8	.18	.119	.045	.101	.044	.006	1.00
Ri della Fibbia	86	1.56	6.70	.078	.012			.137	.007	.254	.007		
Grasso di Froda II	247	.15	2.035	.000	.006	2.00	1.04	.043	.000		.003	.191	(.84)
Grasso di Froda I	314	.141	1.655	/	/	1.10	.09	.050				.030	(.44)
Piz Garviel	45	1.66	4.55	.970	.031			.215	.122	.053	.106		
"	142	1.54	3.65	.474	.020			.248	.075	.070	.064		
Pennines													
Gischihorn	36	.925	3.01	.068	.012			.181	.013	.291	.014		
"	140	.080	.245	.020	.002			.192	.047	.165	.046		
Gh. del Cavagnöö III	318	.016	.194	/	/	.35	.14	.048				.148	1.45
Lago Bianco	315	.691	5.860	.276	/	10.60	.02	.069	.027		.025	.0007	1.05
Fusio	316	.027	.394	/	/	.48	.22	.040				.169	1.02
Aquarossa	312	.165	1.684	/	/	2.65	.25	.058				.035	1.03
Campo Blenio	89	.085	.270	.576	.021			.185	1.223	.060	1.094		
Camperio	321	.115	1.177	.05	/	2.46	.07	.057	.024		.023	.011	1.25

Leere Seite

Blank page

Page vide

Pelvoux Massif

High salinity, with freezing temperatures sometimes lower than the $NaCl$-H_2O eutectic, characterizes the fluids from the Pelvoux massif. This is due to the presence of divalent cations which are expected in fissures located in amphibolites and/or close to the Triassic sediments. Homogenization occurs at about 180° C.

Mont Blanc Massif

Freezing temperatures range from -3.5 to $-7.0°$ C (6 to 10.5 wt% equivalent NaCl, with an average around 8.5 wt%).

In this massif, fissures are located in a quite homogeneous granite, far enough from sediments, so that the values measured here are probably controlled by irreversible leaching of the granite and/or by reactions forming new minerals.

CO_2 concentration is generally quite low (less than 2 wt%). However, it can reach 5 wt% in some places (Tour Noir) or even higher values (Les Courtes, Les Amethystes, POTY 1969). These high concentrations are always related to late fluids in vertical sheared zones.

Homogenization temperatures range between 150° and 210° C, with 36% of the values falling in a narrow range (170 to 185° C) (fig. 1). Higher values are always related to the presence of CO_2, indicated by liquid CO_2 or by CO_2 hydrate formation.
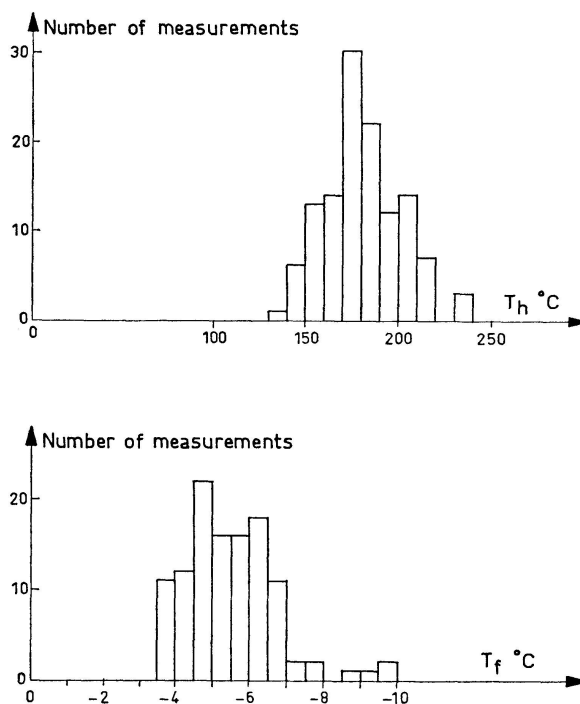
Fig. 1. Frequency distribution diagrams of microthermometric measurements of fluid inclusions from Mont-Blanc massif. Upper diagram: homogenization temperatures; lower diagram: freezing (liquidus) temperatures.

Aar Massif

CO_2 rich inclusions, observed in quartz associated with ankerite, are rare in the Aar massif. The salt content of aqueous solutions varies from zone to zone. It is about 8 wt% NaCl eq. in the area of crystalline schists (North of the massif) and in the eastern part of the massif, though significant differences are present. In the granitic zone of the Central Aar massif (Grimsel area), the salt content is fairly high (11 wt%). It decreases again (5.5 wt%) in the southern gneisses. Some extreme values (western area) can be explained by the proximity of evaporites.

If the CO_2-rich inclusions are not taken into account, the homogenization temperatures fall into a rather narrow range, with an average around 190 to 200° C. This point has been quoted long ago by KOENIGSBERGER and MÜLLER (1906).

Gotthard Massif

The salt content of aqueous solutions from the Gotthard massif is about 7 wt% NaCl eq. The variations are small, with two exceptions (extremely high salt content).

In comparison with the Aar massif, fluid inclusions from Gotthard are quite rich in CO_2. In most of the quartz crystals, inclusions containing more than 10 wt% CO_2 can be seen. Nevertheless, aqueous solutions with two phases are still dominant; they are more recent than many of the CO_2-rich fluids.

The homogenization temperatures of three-phase inclusions range between 250 and 295° C.

Pennines

The salt content is about 6 wt% NaCl eq. It is quite constant except in the youngest inclusions where it decreases considerably. The very high salt content at Camperio might be related to a gypsum deposit in this area (inclusions with halite crystals have been found there).

The Pennines are even richer in CO_2 than the Gotthard massif. Three-phase inclusions with a density of CO_2 above the critical value (0.475 g/cc) are common. But 3-phase inclusions with a density of CO_2 lower than 0.475 g/cc and 2-phase inclusions are also abundant. The CO_2 content decreases with time, and the youngest inclusions contain only a small amount, if any, of this component.

The homogenization temperatures of 3-phase inclusions range from 260 to 360° C. The average value is much higher than in the Gotthard and Aar massives. The low homogenization temperatures recorded in 2-phase inclusions occuring in "needle quartz" from Gh. del Cavagnöö (208° C) and Paltano (220° C), support field evidence which indicate that these crystals belong to the latest crystallization event in the area.

II. Chemical Analyses of Leachates

Seventy nine chemical analyses of fluid inclusions were performed, using the procedure proposed by ROEDDER (1963), with a few improvements. The analyzed ions are K, Na, Ca, Mg and, for 27 samples, Cl and SO_4.

Preparation of the Samples

Cleaning the samples was carried out as follows:

— Immersion for one hour in boiling concentrated high purity nitric acid (Merck 454).
— Immersion for one hour in boiling distilled and deionized water (DDW).
— Immersion for five days in a continuously stirred mixture of DDW and anionic + cationic resins. This step is of critical importance: a duration of less than 5 days yields bad blanks and unreliable results.

After cleaning, each sample was inserted into a stainless steel tube (Sandvik 3 R 12 – OD 20 mm – length 140 mm) closed at one end. This tube was previously cleaned by immersion during one hour in boiling nitric acid, and another hour in boiling DDW.

Crushing and Leaching

Crushing was performed with a 7 Kbar press, and the powdered sample leached with DDW on a Millipore assembly (Pyrex funnel and base, stainless steel filter support screen, 47 mm filter, 0.45 μm) to give 60 ml of solution.

Owing to the low concentration values found in the leachates (a few hundreth of a ppm to a maximum of 15 ppm for most of the samples), the possibility of contamination was seriously considered. A blank was made for each sample in the following way: just before crushing, DDW was poured into the stainless steel tube containing the sample, and this water was then passed through the filter assembly.

All those steps, from cleaning the surfaces with water and resins to obtaining the bottle of leachate, were performed in a room exclusively devoted to this purpose.

Analytical Methods

K, Na, Ca and Mg were analyzed with a Perkin-Elmer 303 atomic absorption apparatus with digital concentration readout. Sensitivity of determinations is a few thousands of a ppm for all those elements, and accuracy is believed to be close to one hundreth of a ppm.

Concentrations in the blanks were usually less than a few thousands of a ppm and were considered perfect in this case. Sometimes they were in the 0.01–0.1 ppm range. When they were equal to or more than 0.1 ppm, contamination was considered to be too large. This occurred in six out of the 79 analyses. However, the results were kept because the concentrations in the six corresponding leachates were high enough.

Chloride was analyzed with a colorimetric method, using ferric ammonium sulfate and mercuric thiocyanate as indicated by ROEDDER (1963). This method allows determinations down to 0.01 ppm Cl and works fairly easily in routine.

Sulfate determinations (methylene blue colorimetric method) were more difficult. As

suggested by ROEDDER (1963) the procedure of JOHNSON and NISHITA (1952) was used first. But the procedure described by GUSTAFSSON (1959) appears to yield more reproducible results, and later analyses (312 and after) were done by that method. Sensitivity is 0.01 ppm and accuracy is believed to be close to 0.05 ppm.

RESULTS

Only a few of the significant components of the solutions were analyzed. H^+, Li^+, Fe, HCO_3^- and F^- are probably the most important ions not looked for. Since the quantity of water in the sample was not determined, the actual concentration of individual ions in the original fluid can be estimated through microthermometry results.

On the other hand ratios between analyzed cations and anions are known with good accuracy for most samples. The atomic ratios: K/Na, Ca/Na, Mg/Ca, $Ca + Mg/K + Na$, SO_4/Cl and the balance of charges between analyzed anions and analyzed cations are especially significant.

It should be noted also that the terms "ion", "cation" and "anion" refer to a theoretical totally ionized aqueous solution. This does not mean that those components were actually present as simple ions at the time of quartz growth, or in the analyzed leachates either.

K/Na

The values are clustered by regions on five different frequency distribution diagrams (fig. 2).

The diagram for the Mont Blanc massif shows an especially sharp peak, close to 0.161 and scatter from 0.095 to 0.191.

In order to get such a sharp peak two conditions have been met:

a) solutions have been buffered by some mineral association and we will see that albite and adularia made the buffer;

b) analyses must have been accurate and this is due to the quality of material from the Mont Blanc massif.

The scatter of the results probably has several causes:

— The cavities studied here were probably not formed at exactly the same time, and differences in PT conditions may have been large, leading to different K/Na ratio of the fluid. This point should be important in the Pennines.

— The nature of the anions is known to affect the equilibrium K/Na ratio for a given reaction (IIYAMA, 1970). Most experimental studies were made with chloride as anion. But for example the presence of HCO_3^- (not analyzed in this work) lowers the K/Na ratio. Total concentration and abundance of other cations should not affect the results very much.
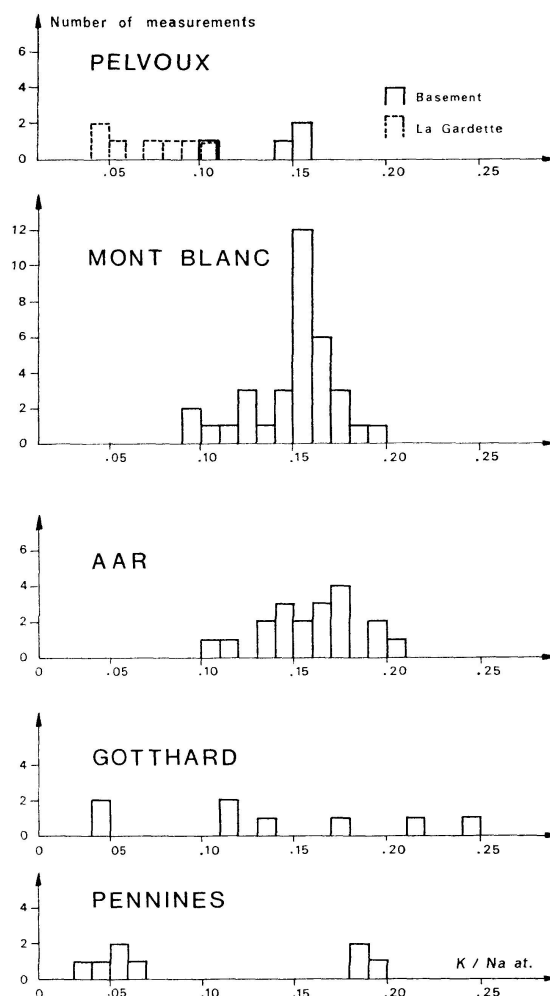
Fig. 2. Frequency distribution diagram of K/Na (atomic ratio) in fluid inclusions from Alpine fissures.

— Errors in chemical analyses do not seem to be a major cause of the scatter of the results since K and Na concentrations are always over 0.3 ppm, the value above which our technique appears to be accurate enough.

In the Pelvoux massif, the data are clustered into two groups. The cluster around 0.15 is related to cavities in the basement not very close to Triassic sediments (Rampe des Commères). The other is related to cavities or veins (La Gardette) in the basement at the contact with Triassic sediments including dolomites.

Here HCO_3^-, not measured but quite likely present, lowers the K/Na ratio as shown by IIYAMA (1970).

In the Aar massif, values are clustered in the manner of the Mont Blanc massif. The peak is not so sharp and this is probably due to the small number of analyses. Its value lies around 0.175, a bit higher than in Mont Blanc (0.161); the maximum found (0.208) is also higher.

The cluster of values for Mont Blanc and Aar suggest that the cavities were made in mainly one process, which is also suggested by field evidence.

In the Gotthard and the Pennines the data are, on the contrary, quite scattered. But the structural history of these regions is more complex. Crystallization in some clefts began with scapolites and ended with zeolites (e.g. at Camperio). Such an evolution in paragenesis suggests a long duration of growth and a decrease of temperature. This has to be reflected in the chemistry of the solutions.

Ca/Na

The values of this ratio are so low (less than 0.05) that no variation can be suspected. There are a few exceptions in the Pelvoux massif, which can be explained by the occurrence of tremolite in veins (fig. 3).

Owing to the large amount of oligoclase that has been incongruently and irreversibly leached during hydrothermal processes, one could expect a higher Ca content in the fluids. The low values measured here indicate that the Ca-content of solutions equilibrated with new-precipitated minerals such as calcite, epidote ... is very low under the P and T conditions that prevailed during the formation of alpine veins.
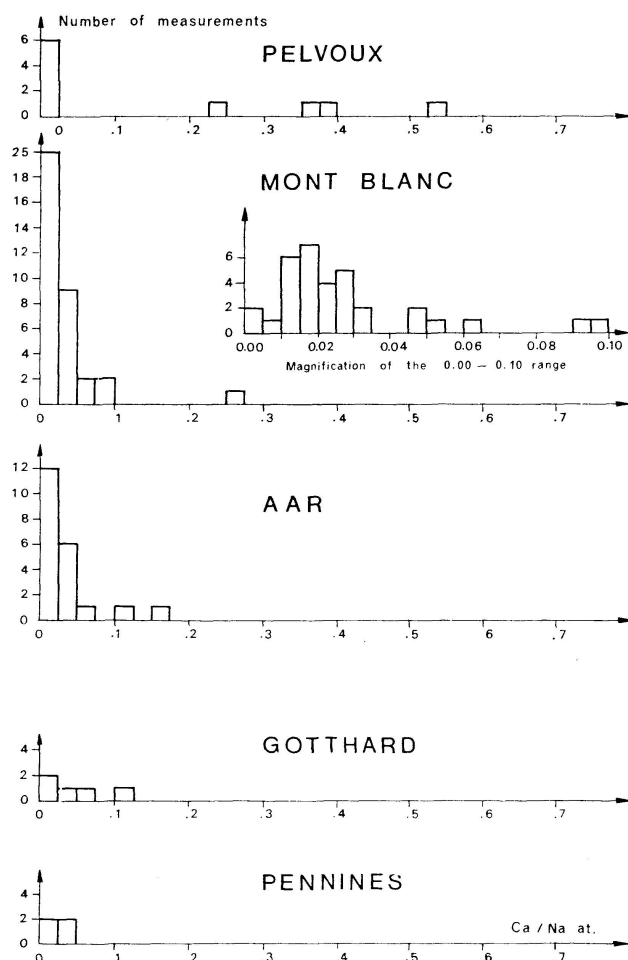
Fig. 3. Frequency distribution diagram of Ca/Na (atomic ratio) in fluid inclusions from Alpine fissures.

Mg/Ca

The results for Mg/Ca ratio are more scattered than those for K/Na. In Pelvoux, Mont Blanc and Aar, two sets of values are found (fig. 4).
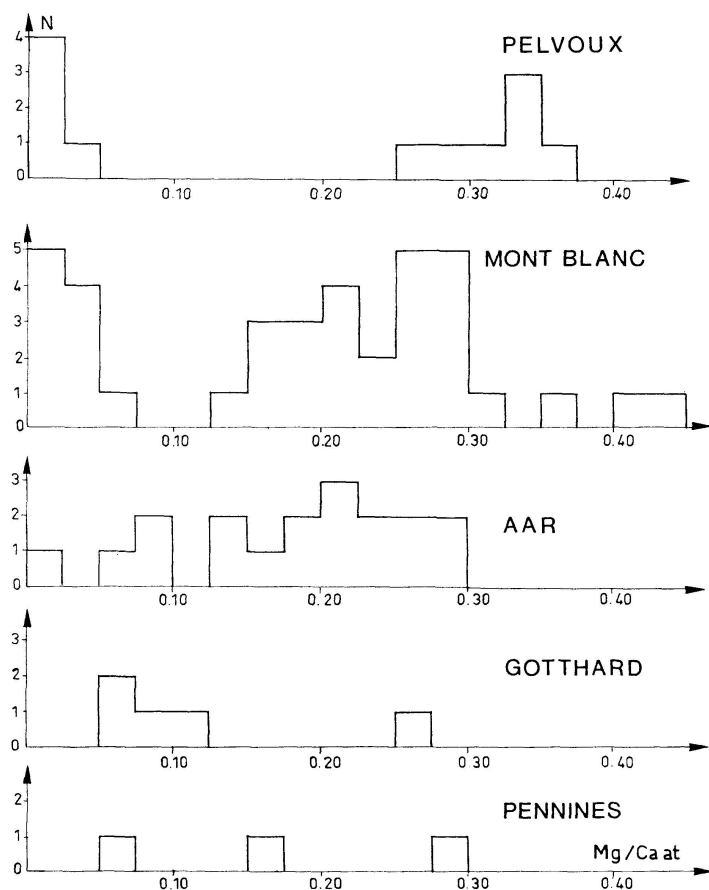
Fig. 4. Frequency distribution diagram of Mg/Ca (atomic ratio) in fluid inclusions from Alpine fissures.

Fig. 5. Relationship between Mg/Ca and K/Na (atomic ratio) in some fluid inclusions from Alpine fissures. Solid symbols: used to calculate the average Mg/Ca; open symbols: not used, because of the low Mg/Ca ratio. Large open symbols: average values from the points shown here for Mg/Ca, and from table IV for K/Na.
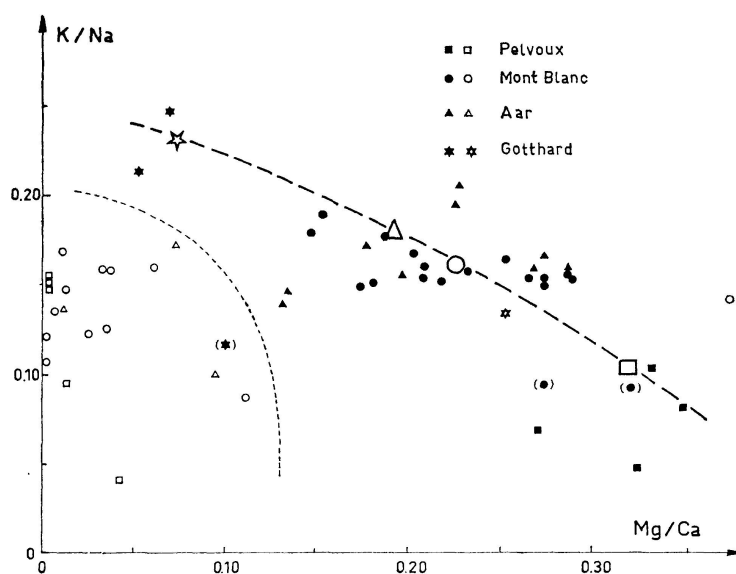
1. 0.01 to 0.10 increasing from Pelvoux to Aar; these low values are found mainly in veins that occur in rocks containing Ca-rich minerals.
2. 0.13 to 0.37, decreasing from Pelvoux to Aar.

One of the most commun buffers of the Mg/Ca ratio in veins is the calcite-dolomite association. Because these two minerals do not always occur at equilibrium in alpine veins, and because Fe-bearing carbonate (ankerite) is usually found in place of dolomite, buffering is imperfect. However, the decrease of Mg/Ca from Pelvoux to Aar (and probably Gotthard) – i.e. with increasing temperature – agrees with experimental data (HOLLAND, 1967). If these values are plotted agains K/Na, a rough trend appears, as seen on fig. 5.

$(Ca + Mg)/(K + Na)$

This ratio does not show any systematic change from one massif to another. Concentration of divalent cations is much lower than concentration of alkalis, generally by two orders of magnitude. However, some values are fairly high (0.1 to 0.5) and this is related to a Ca-rich and $(K + Na)$-poor surrounding; the example of the "Rampe des Commères" is particularly significant, where the fissures are located in amphibolites.

It can be seen that abnormal values of the K/Na ratio are usually obtained when $(Ca + Mg)/(K + Na)$ is high.

SO_4/Cl

In La Gardette vein, close to the Triassic sediments, SO_4/Cl of the fluid phase is amazingly low: 3×10^{-3}. This means that at high T and P only halides will be dissolved and anhydrite will remain. In the Mont Blanc massif values are in the same range, slightly higher in the Aar massif (8×10^{-3}) and much more scattered in the Gotthard and the Pennines $(1 \times 10^{-3}$ to $35 \times 10^{-3})$, with some as high as 190×10^{-3}.

Anions-Cations Charge Balance

The ratio $\sum$ analyzed anions / $\sum$ analyzed cations in equivalent (i. e. $\sum n_A z A^{z-} / \sum n_M z M^{z+}$) is amazingly constant. Out of 25 values, only two are lower than 1.00 (0.98 and 0.96) and two are higher than 1.20 (1.25 and 1.44). More than 50% fall in the range 1.00–1.10; the average value is 1.08.

Since all species were not analyzed, only a tentative interpretation can be made. Of the data that are missing, those concerning Fe and carbonate should be the most important. Because the latter is probably more abundant than the former, the excess of negative charges is still larger than the values obtained above. This excess must be balanced by hydrogen (occuring as H^+ and in acid molecules, complex anions or complex molecules), the concentration of which was therefore rather constant and fairly high in the solutions of alpine veins.

III. Discussion: The Place of Fissures in Alpine Metamorphism

Results given by microthermometry and chemical analyses of leachates may help understanding the formation of alpine fissures and their place in alpine metamorphism.

First, the use of K/Na ratio of fluids buffered by adularia and albite is discussed in terms of geothermometry. Knowing the temperature determined in this way, pressure can be estimated through microthermometry results, using the isochores.

These PT data are used then to estimate depths and to discuss the origin of the fluids.

Use of K/Na Ratio in Fluid Inclusions from Quartz in Equilibrium with Adularia and Albite as a Geothermometer

Equilibrium between two alkali feldspars and an alkali-chloride solution can be written:

$$\text{Orthoclase} + \text{NaCl}_{aq} \rightleftarrows \text{Albite} + \text{KCl}_{aq}.$$
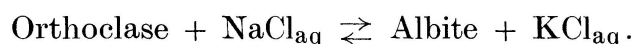
The equilibrium conditions are determined by the following set of equations:

$$\mu_{\text{KCl}_{aq}} - \mu_{\text{NaCl}_{aq}} = \mu_{\text{Or}} - \mu_{\text{Ab}},$$

$$\mu_{\text{Or}} \text{ in K-spar} = \mu_{\text{Or}} \text{ in Na-spar},$$

$$\mu_{\text{Ab}} \text{ in K-spar} = \mu_{\text{Ab}} \text{ in Na-spar}.$$

If m_{KCl} and m_{NaCl} are the molality of total KCl and NaCl in the solution at equilibrium with two feldspars, a relation is calculated:

$$\text{Ln}\frac{m_{\text{KCl}}}{m_{\text{NaCl}}} = f(T, P, a_{ic}, a_{iaq}),$$

where a_{ic} and a_{iaq} are the activities of components other than K and Na in solid phases and in the solution, respectively.

The last equation can be approximated by:

$$\text{Ln}\frac{m_{\text{KCl}}}{m_{\text{NaCl}}} \sim f(T, P).$$

This function has been calculated, using the data from ORVILLE (1963) and HEMLEY (1967) (see appendix I). Fig. 6 gives the corresponding curve.

The uncertainty associated with this curve depends on the uncertainty of the experimental data and on the validity of the various approximations:

1. The only available data consist of 3 values at 2 Kbar, 670, 600, 500° C (ORVILLE, 1963) and 3 values at 1 Kbar, 500, 400 and 300° C (HEMLEY, 1967).

Fig. 6. K/Na atomic ratio in solutions at equilibrium with two alkali feldspars, as a function of temperature. The curves are probably valid in the 1–3 kbar pressure range.
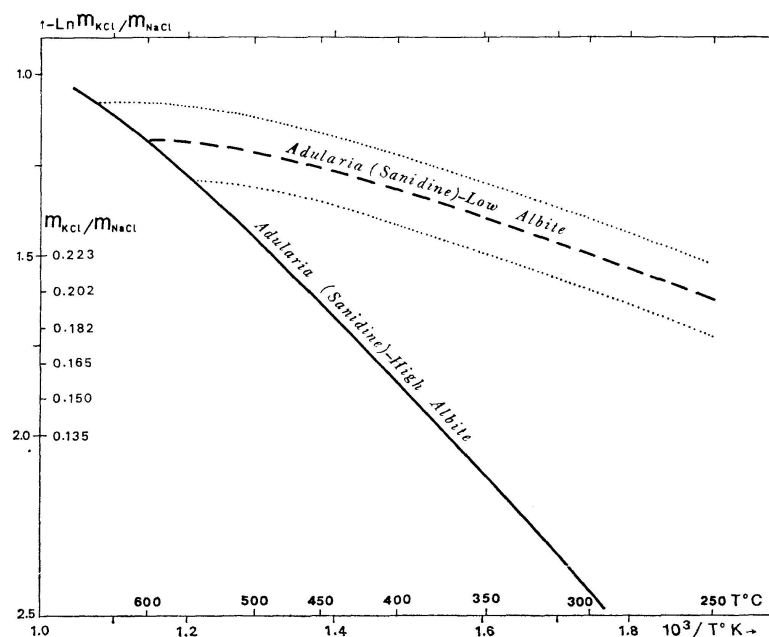
Estimation of the effect of pressure upon the equilibrium is rather difficult, but it seems that, in the pressure range expected for the formation of alpine veins (2 to 3 Kbar), this effect is not very important. Nevertheless, the pressure effect on the equilibrium is a source of possible error.

2. The ratio $\gamma_{KCl}/\gamma_{NaCl}$ (stoichiometric activity coefficients of KCl and NaCl) in solution is approximated as a linear function of $1/T$ (see Appendix I). At low temperatures, the resulting error might be fairly large.

3. The equation of state for a crystalline solution of sanidine has been used in the calculations. The entropy of mixing (and therefore the Gibbs free energy of mixing) of adularia – which is the actual feldspar occuring in the alpine veins – is not known. However, according to WALDBAUM and ROBIE (1971), the differences in these properties between sanidine and adularia must be small.

4. Using theoretical values for the solvus is certainly better than taking actual analyses of coexisting feldspars in explored veins, for those minerals may have re-equilibrated after their formation.

5. The sources of error resulting from neglecting the components other than K and Na must be discussed accurately. These components are mainly divalent cations (Ca^{2+}, Mg^{2+}, Fe^{2+} and Fe^{3+} ...), anions such as SO_4^{2-}, HCO_3^- and various undissociated complexes.

Analyses of fluid inclusions show that concentrations of Ca^{2+}, Mg^{2+} and SO_4^{2-} are quite low in solutions, and it is probably the same for other components. Thus, it is unlikely that these components will significantly disturb the nearly ideal mixing of KCl-NaCl aqueous solution.

In the solid phases calcium changes the activities of the feldspar end-members. Owing to the very low anorthite content of the albites dealt with, this effect can be neglected.

FOURNIER and TRUESDELL (1973) discussed the effect of calcium upon equilibrium conditions. The general equation they give (eq. 9, p. 1264) is relevant only when the solution is "semi-buffered" by (Na, K, Ca) minerals (adularia-plagioclase for example). As soon as equilibrium is assumed between the solution and two non-calcic alkali feldspars, and even if other calcic minerals are precipitated, calcium is not involved in the equilibrium constant.

The original Na-feldspar in the rocks surrounding the veins in Mont Blanc and Aar massives is usually an oligoclase. But the co-occurrence of albite in those rocks clearly indicates an irreversible and incongruent dissolution of the plagioclase. This Ca-bearing feldspar feeds the solution, yielding solute species which, in turn, can be precipitated as adularia, albite, muscovite, epidote, calcite ... Of course, our derivations and interpretations assume local equilibrium between solution and new-formed minerals (particularly adularia and albite, which is the only Na-feldspar occurring in the veins) but the same assumption cannot be defended for the system plagioclase-solution (see, for instance, HELGESON 1967, 1968, 1969).

Structural state of albite at the time of growth

There is very little doubt about the nature of K-feldspars equilibrated with hydrothermal solutions in both experiments and natural veins (sanidine-like structural state). On the other hand, there is no evidence clearly indicating the state of Na-feldspars under the same conditions. Synthetizing low-albite requires special conditions, such as high alkalinity, etc. ..., and many facts show that albite can reasonably be assumed to crystallize in a disordered state during hydrothermal experiments.

Albite crystals in veins are now ordered. Taking in account the similarities (concentrations of solutes in solutions, for instance) between natural growth and hydrothermal experiments, the effect of water upon the structural state of synthetic albite (MARTIN, 1969) and the systematic disordered state of hydrothermally grown K-feldspars, one can expect that natural hydrothermal albite grew first as high albite. Even if ordering is a fast process, the growing albite can be imagined with a more or less ordered core, coated by a disordered rim in equilibrium with the solution (BROWN, W., personal communication).

In order to test this hypothesis, an approximate curve has been calculated for the adularia (sanidine) – low albite – solution equilibrium (see appendix II, fig. a 6). Using both curves of fig. 6 and the example of the cavity Les Courtes I (Mont Blanc Massif) the following results are obtained:

— Characteristics of the fluids:

Homogenization temperature, 185° C.

Salinity, 7.7% wt (NaCl) for a pure aqueous solution (no CO_2 present).

K/Na at = 0.170.

On the adularia-high albite curve this K/Na ratio gives an equilibration temperature of 420° C and, plotting this value on the isochore (LEMMLEIN and KLEVTSOV, 1961), pressure appears to be close to 2850 bars.

Using the Adularia-low albite curve, an equilibration temperature lower than 200° C is obtained (235° C if the maximum probable error in enthalpy measurements of low- and high-albite is taken into account). In those two cases, using the Adularia-low albite curve, pressure would have been either close to vapour pressure or between 500 and 600 bars. Boiling having never been observed for pure aqueous solutions, vapour pressure is excluded. Obviously the other value is much too low and cannot be defended. The low albite-adularia curve also gives a rather low temperature for green schist facies minerals. But results are still worse for pressure.

Radiometric dating of fissure minerals (K-Ar and Rb-Sr) from the Mont Blanc massif (LEUTWEIN et al. 1970) gives a value close to 15 my. Even if this age is a cooling one, it can be used to get a rough idea of the amount of cover over fissure minerals at the time of their growth. CLARK and JÄGER (1969), using geochronologic and heat flow data, evaluated the rate of erosion in the Alps at 0.7 ± 0.3 mm/year i.e. 0.7 km/my. This value means an erosion of 10.5 km overburden, over cavities, in 15 my. If fluid pressure was close to rock pressure (average rock density 2.7) pressure would have been around 2850 bars. The agreement of this pressure with that calculated above using the adularia-high albite-solution geothermometer is remarkable.

In conclusion it seems reasonable to assume that the sodium feldspar at equilibrium with the solution during its growth was disordered. Thus, using the calculated adularia – high albite – solution curve fig. 6, growth temperatures can be calculated from K/Na ratios of leachates. From microthermometry results (homogenization and freezing temperatures) a PT relationship (constant density: isochore) is determined, which in turn, can be used to calculate the pressure.

Temperatures, Pressures and Depths of Formation of Alpine Fissures

Pressure and depth data calculated in this manner are given for a number of alpine cavities (table V). The number was limited by two requirements: feldspars must have been stable in the cavity or nearby in the country rock, and isochores must be known with good accuracy. This is only possible in the case of pure aqueous solutions. Fluids containing more than a small amount

Table V. *Estimated temperature and pressure of formation of some alpine fissures*

	K/Na	Tempera-ture[1])	Homogeni-zation Temp.[2])	NaCl W %[2])	Pressure bars	Depth km[3])
Pelvoux						
Alpe d'Huez	0.106	335	183	17	1700	6.3
Mont Blanc						
Trient	0.154	400	170	7.8	2850	10.5
Charlet Straton	0.154	400	195	8	2400	8.9
Tour Noir	0.159	410	215	8.5	>2300	>8.5
Les Courtes I	0.170	420	185	7.7	2850	10.5
II	0.166	415	183	8.0	2800	10.4
III	0.171	420	175	7.3	3000	11.1
Grands Montets	0.159	410	182	7.8	2750	10.2
Rachasses	0.153	400	196	9.4	2400	8.9
Talèfre	0.161	410	190	9.0	2600	9.6
Pierre Joseph I	0.161	410	200	9.0	2500	9.3
Les Périades	0.171	420	160	9.2	3200	11.9
Les Mottets	0.162	410	196	8	2500	9.3
Average	0.161	410	178	8	2800	10.4
Aar						
Kammegg	0.158	405	182	4.8	2750	10.2
Tiefengletscher \ Gletschhorn /	0.191	450	208	9.5	2800	10.4
Gletsch	0.184	440	207	6.7	2800	10.4
Gerstengletscher	0.168	420	187	11.8	2800	10.4
Average central zone	0.179	430	196	8	2800	10.4
Gotthard						
Ri della Fibbia	0.137	>380	258	5.8	>1400	> 5.2
Piz Garviel	0.231	>505	252	9.0	>2700	>10
Pennines						
Gischihorn	0.186	445	265	4.2	2050	7.6

[1]) from K/Na curve fig. 6.
[2]) from Table I.
[3]) assuming $P_{fluids} = P_{solids}$ and for a rock density of 2.7.

of CO_2 (5 weight %) must be excluded. In addition to the effect on the isochores a high CO_2 content may disturb the equilibrium constant of the system two feldspars – aqueous solutions.

Temperatures are high and show, as do radiometric data (table I), that alpine fissures did not appear very late in alpine metamorphism. This is not surprising. In cavities like Camperio for instance, the succession of minerals began with scapolites. In the Mont Blanc massif temperatures were not easy to estimate using only mineral associations. Data given here show that the process of fissure formation was rather unique in temperature conditions and probably unique also in time of formation. It seems to be the same in the Aar massif, at least in the central zone. Kammegg shows a lower temperature than in the central zone and this was expected from its northern location.

In the Gotthard massif Piz Garviel gives the highest recorded temperature = 505° C. But many other values listed in tables III and IV indicate a more complicated history of fissures in this area, as well as in the Pennines.

Pressures are well clustered for the Mont Blanc massif. If fluid pressure is taken to be equal to rock pressure, the depth of formation may be estimated assuming a density of 2.7 for the average rock (table V). These calculations give values close to 9 to 10 km. Such a depth is quite reasonable if we consider the thickness of the Nappe de Morcles which was probably over the Mont Blanc massif at the time of formation of the fissures. These data suggest also that fluid pressure was probably very close to rock pressure. Opening of fissures would require such an identity of fluid and solid pressures. If the former is much less than the latter, depth would be much higher which is difficult to admit.

The constancy of pressure and depth (2.5 to 3 Kbar, 9.5 to 11 km) all over the Mont Blanc and Aar massifs indicates that this region was at the same structural level at the time of formation of the fissures. The differences of temperatures, from 400° C in the Mont Blanc and northern part of the Aar, to 450° C in the central zone of Aar, are thus not related to the depth of burying and can be tentatively interpretated by the occurence of a hot center probably located in the central part of the Pennines.

Gradients at the time of fissure formation calculated from those data are the following:

Average Mont Blanc		37°/km
Aar, Kammegg		37°/km
Central zone		42°/km
Gotthard	Piz Garviel	< 48°/km
Pennines	Gischihorn	55°/km

These values are average values and it should be kept in mind that the gradients were probably not identical in granites or gneisses and in overlying sediments.

Origin of Fluids

It appears from this work that water is the major component of the fluid phase in alpine veins.

Because the rocks located below the levels investigated here should be quite dehydrated, the origin of the water must be found in overlying and surrounding sediments, or in circulation from the surface. Although the migration of meteoric or connate water has been demonstrated in many places by various authors, mainly in studies on oxygen and hydrogen isotopes, the same process has not been expressed yet for the Alps, as far as we know. If

the hypothesis of participation of meteoric water is correct, that means that circulation down to more than 10 km is possible.

Two kinds of occurrences of CO_2 have been recognized.

CO_2 occurs as an early fluid (Pennines Gotthard, and to a lesser extent, Aar). This early CO_2 was not found in Pelvoux and Mont Blanc massives. Its concentration decreases during the progressive opening of fissures. This indicates a decrease of temperature with time, a fact firmly established by both the succession of minerals and fluid inclusions studies. This early CO_2 could be related to the metamorphism of carbonate bearing rocks.

High concentrations of CO_2 are also found in late fluids, all over the Alps. This CO_2-rich fluid is generally responsible for the skeletal habit of quartz crystals (sceptres). No decarbonation can be invoked for supplying CO_2 at that time. The origin of a CO_2-rich fluid is more likely related to the unmixing of a previously homogeneous CO_2-H_2O mixture as the whole rock-mass was cooling.

APPENDIX I

Sanidine (Adularia) - High Albite-Solution Equilibrium. General Relations

The equilibrium between a KCl-NaCl aqueous solution and two alkali feldspars can be described by the reaction:

$$Or^{Or} + Na^+ \rightleftarrows Ab^{Ab} + K^+ \quad \text{or} \quad Or^{Or} + NaCl \rightleftarrows Ab^{Ab} + KCl.$$

Or^{Or} and Ab^{Ab} represent respectively the orthoclase end-member in the K-rich feldspar and the albite end-member in the Na-rich feldspar.

The equilibrium condition is:

$$\mu_{KCl} - \mu_{NaCl} = \mu_{Or}^{Or} - \mu_{Ab}^{Ab} \tag{1}$$

with

$$\mu_{Or}^{Or} = \mu_{Or}^{\cdot} + R\,T\,Ln\,a_{Or}^{Or}, \tag{2}$$

$$\mu_{Ab}^{Ab} = \mu_{Ab}^{\cdot} + R\,T\,Ln\,a_{Ab}^{Ab}. \tag{3}$$

$\mu_{Or}^{\cdot}$ and $\mu_{An}^{\cdot}$ are the chemical potentials (Gibbs free energies) of pure orthoclase and pure albite.

The chemical potentials of KCl (aqueous) and NaCl (aqueous) can be written (see, for instance, DENBIGH, 1968, p. 306):

$$\mu_{KCl} = \mu_{K^+}^* + \mu_{Cl^-}^* + R\,T\,Ln\,\gamma_{KCl}\,m_{KCl}, \tag{4}$$

$$\mu_{NaCl} = \mu_{Na^+}^* + \mu_{Cl^-}^* + R\,T\,Ln\,\gamma_{NaCl}\,m_{NaCl}. \tag{5}$$

μ_i^* is the chemical potential of the species i in the usual reference state. The symbols m_{KCl} and m_{NaCl} refer to the total molality of the electrolytes, and γ_{KCl} and γ_{NaCl} are the stoechiometric activity coefficients of KCl and NaCl in the solution.

Combining equations (2), (3), (4), (5) with (1), and rearranging:

$$\text{Ln}\,\frac{m_{KCl}}{m_{NaCl}} - \text{Ln}\,\frac{a_{Or}^{Or}}{a_{Ab}^{Ab}} = -\frac{\mu_{K^+}^* - \mu_{Or}^{\cdot} - (\mu_{Na^+}^* - \mu_{Ab}^{\cdot})}{RT} - \text{Ln}\,\frac{\gamma_{KCl}}{\gamma_{NaCl}} \tag{6}$$

and with

$$\mu_{K^+}^* - \mu_{Or}^{\cdot} - (\mu_{Na^+}^* - \mu_{Ab}^{\cdot}) = (\varDelta\,G)^{P,\,T}: \tag{7}$$

$$\text{Ln}\,\frac{m_{KCl}}{m_{NaCl}} - \text{Ln}\,\frac{a_{Or}^{Or}}{a_{Ab}^{Ab}} = -\frac{(\varDelta\,G)^{P,\,T}}{RT} - \text{Ln}\,\frac{\gamma_{KCl}}{\gamma_{NaCl}}. \tag{8}$$

Activity coefficients in the solution

The activity coefficients γ_{KCl} and γ_{NaCl} take care not only of the non-ideality of the solution and the choice of the molality scale, but also of the occurrence, in the solution, of undissociated neutral complexes KCl_0 and $NaCl_0$.

Data from ROBINSON (1961), STERN and ANDERSON (1964), GAMMON, BORCSIK and HOLLAND (1967), WELLMAN (1970), indicate that aqueous solutions of KCl and NaCl (with a constant total molality) mix ideally, or very nearly so, in a wide range of temperature and pressure. Therefore, it can be assumed that, in equation (8), the part of

Fig. a1. Conventional dissociation constants of KCl and NaCl in aqueous solution, at 1 and 2 kbar. Calculated from data of Quist and Marshall (1968), Ritzert and Franck (1968) and Burnham et al. (1970).
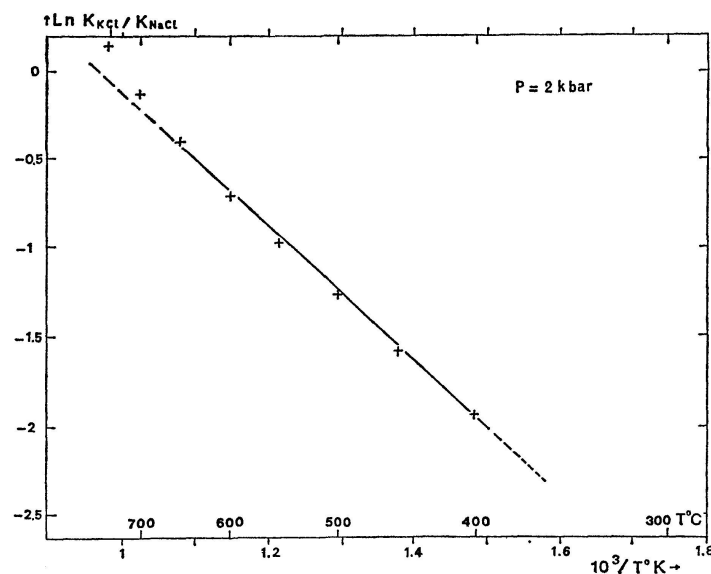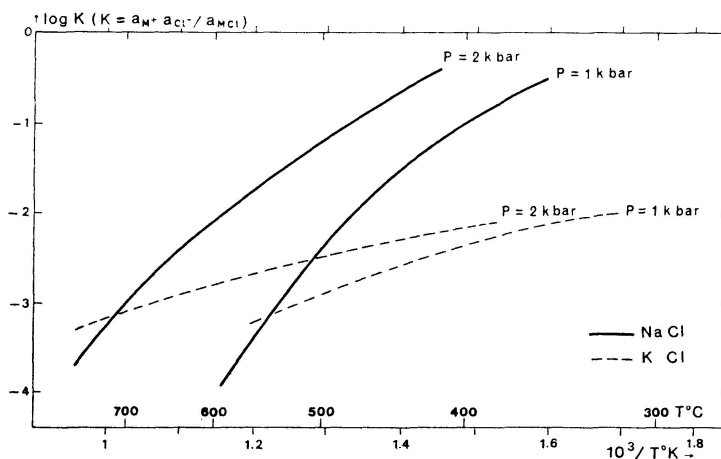
Fig. a2. Variations of the ratio of conventional dissociation constants of KCl and NaCl with temperature at 2 kbar total pressure.

$\gamma_{KCl}/\gamma_{NaCl}$ that does not take in account the partial dissociation of the electrolytes is constant.

Fig. a1 and a2 have been calculated from the data of QUIST and MARSHALL (1968) and RITZERT and FRANCK (1968) on the conventional dissociation constants K_{KCl} and K_{NaCl} of KCl and NaCl and the specific volume of water (BURNHAM et al., 1970). These figures show that, at constant pressure (P = 2 kbar), the value of $Ln(K_{KCl}/K_{NaCl})$ can be approximated by a linear fonction of $1/T$, at least in between 300° C and 650° C.

Now, if the variation (ΔC_p) is neglected in the calculation of (ΔG) (eq. 7), the quantity $(\Delta G)/RT$ is a linear fonction of $1/T$. Hence, the right side of eq. (8) is also a linear fonction of $1/T$ and we can write:

$$Ln \frac{m_{KCl}}{m_{NaCl}} - Ln \frac{a_{Or}^{Or}}{a_{An}^{An}} \approx \alpha + \frac{\beta}{T}, \tag{9}$$

where A and B are constants.

Activities of components in the feldspar phases

The chemical potential of the orthoclase end-member in an alkali feldspar can be written:

$$\mu_{Or} = \mu_{Or,id} + \mu_{Or,ex}$$

or

$$\mu_{Or}^{\cdot} + R\,T\,Ln\,\gamma_{Or}\,N_{Or} = \mu_{Or}^{\cdot} + R\,T\,Ln\,N_{Or} + \mu_{Or,ex}. \tag{10}$$

$\mu_{Or}^{\cdot}$ is the Gibbs free energy of pure orthoclase, at the same P and T. N_{Or} is the molar fraction $K/K+Na$ in the feldspar, and γ_{Or} is the activity coefficient of orthoclase in the same feldspar. From (10) we get

$$\gamma_{Or} = e^{\mu_{Or,ex}/RT}. \tag{11}$$

The excess chemical potential $\mu_{Or,ex}$ is (Gibbs-Duhem equation):

$$\mu_{Or,ex} = G_{ex} - N_{Ab} \frac{\partial G_{ex}}{\partial N_{Ab}}. \tag{12}$$

Assuming a regular assymetric mixture model for the feldspars (THOMPSON, 1967), the excess free energy G_{ex} is:

$$G_{ex} = A\,N_{Ab}\,N_{Or}^2 + B\,N_{Or}\,N_{Ab}^2. \tag{13}$$

A and B are the Margules parameters. They are independant of composition, and are constant at given P and T.

Calculating $\dfrac{\partial G_{ex}}{\partial N_{Ab}}$ and reporting this value and G_{ex} in (12) gives:

$$\mu_{Or,ex} = (2\,A - B)\,N_{Ab}^2 + 2\,(B - A)\,N_{Ab}^3 \tag{14}$$

and also

$$\mu_{Ab\ ex} = (2\,B - A)\,N_{Or}^2 + 2\,(A - B)\,N_{Or}^3. \tag{15}$$

Using the equation of state given by WALDBAUM and THOMPSON (1969), we get directly

$$A = 6326.7 + 0.0925\,P - 4.6321\,T, \tag{16}$$

$$B = 7671.8 + 0.1121\,P - 3.8565\,T. \tag{17}$$

From the same authors, we get also the composition $N_{Or}^{(Ab)}$ and $N_{Ab}^{(Or)}$ of two coexisting feldspars versus T and P, i.e. the solvus values (WALDBAUM and THOMPSON, 1969, table 1).

Activities of the feldspars and $Ln\,a_{Or}^{Or}/a_{Ab}^{Ab}$ at 1 and 2 kbar are given below (table a1 and fig. a3 and a4).

Table a1

T °C	K-rich feldspar		Na-rich feldspar		$-\mathrm{Ln}\,\dfrac{a_{Or}^{Or}}{a_{Ab}^{Ab}}$
	N_{Or}^{Or}	a_{Or}^{Or}	N_{Ab}^{Ab}	a_{Ab}^{Ab}	
P = 1 kb					
662	0.333	0.649	0.667	0.892	0.318
606	0.585	0.713	0.855	0.917	0.253
512	0.762	0.812	0.935	0.952	0.159
428	0.866	0.886	0.969	0.974	0.094
335	0.940	0.946	0.988	0.989	0.045
241	0.980	0.981	0.997	0.997	0.016
195	0.990	0.990	0.999	0.999	0.008
P = 2 kb					
675	0.333	0.649	0.667	0.893	0.318
648	0.506	0.680	0.807	0.905	0.285
599	0.628	0.734	0.877	0.925	0.232
504	0.790	0.831	0.944	0.957	0.142
391	0.908	0.919	0.980	0.982	0.066
296	0.963	0.966	0.993	0.993	0.028
201	0.990	0.990	0.999	0.999	0.008

Fig. a3. Activities of orthoclase and albite end members in coexisting alkali feldspars at temperatures up to the critical temperature and pressure of 1 to 2 kbar.
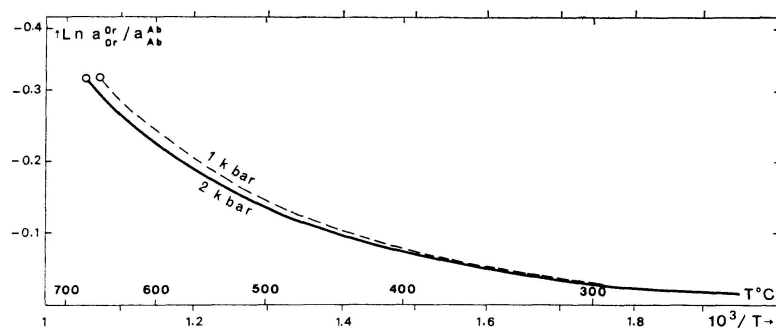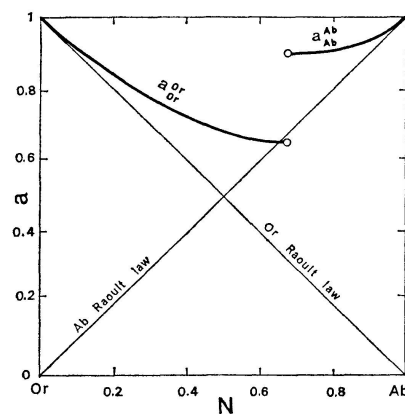
Fig. a4. Negative logarithm of the ratio of activities of orthoclase and albite in coexisting alkali feldspars as a fonction of temperature, at 1 and 2 kbar.

Smoothing the experimental data

The values of the coefficients α and β in equation (9) can be calculated from the experimental data of ORVILLE (1963) and HEMLEY (1967) at 2 and 1 kbar (table a2).

Table a2

T °C	$10^3/T$ °K	m_{KCl}/m_{NaCl}	$\mathrm{Ln}\ m_{KCl}/m_{NaCl}$	$-\mathrm{Ln}\ a_{Or}^{Or}/a_{Ab}^{Ab}$	$\mathrm{Ln}\ m_{KCl}/m_{NaCl}-\mathrm{Ln}\ a_{Or}^{Or}/a_{Ab}^{Ab}$
670	1.060	0.351[1])	-1.05	0.31	-0.74
600	1.145	0.302[1])	-1.20	0.23	-0.97
500	1.294	0.227[1])	-1.48	0.135	-1.345
500	1.294	0.232[2])	-1.46	0.145	-1.315
400	1.486	0.161[2])	-1.82	0.08	-1.74
300	1.745	0.086[2])	-2.45	0.03	-2.42

[1]) ORVILLE, 1963, 2 kb, mica-free.   [2]) HEMLEY, 1967, 1 kb, with muscovite.

The values of $\mathrm{Ln}\ m_{KCl}/m_{NaCl} - \mathrm{Ln}\ a_{Or}^{Or}/a_{Ab}^{Ab}$ plotted against $1/T$ fit a straight line (fig. 5). Actually, two lines can be calculated

1. one using ORVILLE's data only (P = 2 kb),
2. the other using the data of both Orville and Hemley, assuming that the difference in pressure (1 and 2 kb) yields a variation which can be neglected.

From thoses straight lines, the smoothed equilibrium cuves giving $\mathrm{Ln}\ m_{KCl}/m_{NaCl}$ versus $1/T$ can be easily computed (fig. a5).

Fig. a5. Construction of the smoothed equilibrium curve in the system: two alkali feldspars - NaCl - KCl aqueous solution. Solid lines: Calculated from both Orville and Hemley data, broken lines: calculated from Orville data only (P = 2 kbar).

APPENDIX II

Adularia - Low Albite - Solution Equilibrium

Equation (8) (appendix I) refers to equilibria between two feldspars and a solution, whatever the structural states of the feldspars are.

Using the subscripts H and L to indicate adularia – high albite and adularia – low albite equilibria, respectively, it can be written, hence:

$$Ln\left(\frac{m_{KCl}}{m_{NaCl}}\right)_H - Ln\left(\frac{a_{Or}^{Or}}{a_{Ab}^{Ab}}\right)_H = -\frac{(\varDelta G_H)^{P,\,T}}{RT} - Ln\left(\frac{\gamma_{KCl}}{\gamma_{NaCl}}\right)_H, \tag{1}$$

$$Ln\left(\frac{m_{KCl}}{m_{NaCl}}\right)_L - Ln\left(\frac{a_{Or}^{Or}}{a_{Ab}^{Ab}}\right)_L = -\frac{(\varDelta G_L)^{P,\,T}}{RT} - Ln\left(\frac{\gamma_{KCl}}{\gamma_{NaCl}}\right)_L. \tag{2}$$

Substracting (1) from (2) and remembering that $\gamma_{KCl}/\gamma_{NaCl}$ is constant (at given P and T) with the assumption of ideal mixing of KCl and NaCl in aqueous solutions:

$$\left(Ln\frac{m_{KCl}}{m_{NaCl}} - Ln\frac{a_{Or}^{Or}}{a_{Ab}^{Ab}}\right)_L - \left(Ln\frac{m_{KCl}}{m_{NaC}} - Ln\frac{a_{Or}^{Or}}{a_{Ab}^{Ab}}\right)_H = -\frac{(\varDelta G_L)^{P,\,T} - (\varDelta G_H)^{P,\,T}}{RT}. \tag{3}$$

We know (equation 7, appendix I) that:

$$\varDelta G = \mu_{K^+}^* - \mu_{Na^+}^* - (\mu_{Or}^\cdot - \mu_{Ab}^\cdot).$$

Therefore: $(\varDelta G_L)^{P,\,T} - (\varDelta G_H)^{P,\,T} = \mu_{Ab\,L}^\cdot - \mu_{Ab\,H}^\cdot = -(\varDelta G_{Ab\,L \to H})^{P,\,T}.$

And with (3):

$$\left(Ln\frac{m_{KCl}}{m_{NaCl}} - Ln\frac{a_{Er}^{Or}}{a_{Ab}^{Ab}}\right)_L - \left(Ln\frac{m_{KCl}}{m_{NaCl}} - Ln\frac{a_{Or}^{Or}}{a_{Ab}^{Ab}}\right)_H = \frac{(\varDelta G_{Ab\,L \to H})^{P,\,T}}{RT}. \tag{4}$$

Because of the lack of knowledge of the excess entropy of mixing of low albite – microcline solid solutions, the quantity

$$Ln\left(\frac{a_{Or}^{Or}}{a_{Ab}^{Ab}}\right)_H \bigg/ \left(\frac{a_{Or}^{Or}}{a_{Ab}^{Ab}}\right)_L$$

cannot be computed. However, according to WALDBAUM and ROBIE (1971), it seems that the structural state of K-Na feldspars has little effect on their mixing properties. Therefore, it can be approximated:

$$\left(\frac{a_{Or}^{Or}}{a_{Ab}^{Ab}}\right)_H \bigg/ \left(\frac{a_{Or}^{Or}}{a_{Ab}^{Ab}}\right)_L \approx 1$$

and $$\left(Ln\frac{m_{KCl}}{m_{NaCl}}\right)_L - \left(Ln\frac{m_{KCl}}{m_{NaCl}}\right)_H = \frac{(\varDelta G_{Ab\,L \to H})^{P,\,T}}{RT}. \tag{5}$$

If we assume a first-order transition for the reaction Ab L $\rightleftarrows$ Ab H, the Gibbs free energy of reaction $(\varDelta G_{Ab\,L \to H})^{P,\,T}$ can be computed from the following data:

* $(\varDelta H)^{1,298} = 2.6 \pm 0.3$ KCal (WALDBAUM and ROBIE, 1971).

* The transition Ab L $\rightleftarrows$ Ab H is likely to occur at about 600° C (McCONNEL and McKIE, 1960; HOLM and KLEPPA, 1968).

* $(H_T - H_{298})$ and $(S_T - S_{298})$ are from ROBIE and WALDBAUM (1968).

The entropy of transition, calculated from those data (($\Delta S_{Ab\,L} \to H)^{1,298} \approx 2.55$ e.u.) is significantly lower than the entropy given in ROBIE and WALDBAUM (1968), i.e. 4.47 e.u. However, we get at 700° C a value of about 3.9 e.u., which agrees with the values estimated by HOLM and KLEPPA (1968).

With $(\Delta V_{Ab\,L \to H}) \approx 0.0086$ cal/bar, the following values of $(\Delta G_{Ab\,L \to H})$ are computed (Table a3).

Table a3

T °K	$(\Delta H)^{1,\,T}$ cal	$(\Delta S)^{1,\,T}$ eu	$(\Delta G)^{1,\,T}$ cal	$(\Delta G)^{2\,kb,\,T}/rt$
500	2837	3.15	1262	1.28
600	2954	3.36	938	0.80
700	3072	3.53	601	0.44
800	3189	3.67	253	0.17
900	3306	3.80	-114	-0.05

The uncertainty of $(\Delta G)/RT$ is:

$$\delta \left(\frac{\Delta G}{RT}\right) = \frac{1}{R} \left(\frac{\delta(\Delta H)}{T} + \delta(\Delta S)\right).$$

With $\delta (\Delta H) = 300$ cal, $\delta (\Delta S) = 0.15$ eu, $\delta (\Delta G/RT)$ varies from 0,24 at 900° K to 0.37 at 500° K. Those are large numbers, but the uncertainty of $\Delta G/RT$, and therefore on $\mathrm{Ln}\,(m_{KCl}/m_{NaCl})$ can be reduced, owing to the following considerations:

* The value of $(\Delta H)^{1,298} = 2.6$ Kcal has been reproduced several times within less than 100 cal (HOLM and KLEPPA, 1968; HOVIS et al., 1970; WALDBAUM and ROBIE, 1971), and the uncertainty of ± 300 cal is certainly overestimated.

* The transition low albite – high albite is unlikely to occur at temperatures lower than 490° (C and probably 550° C) or higher than 670° C.
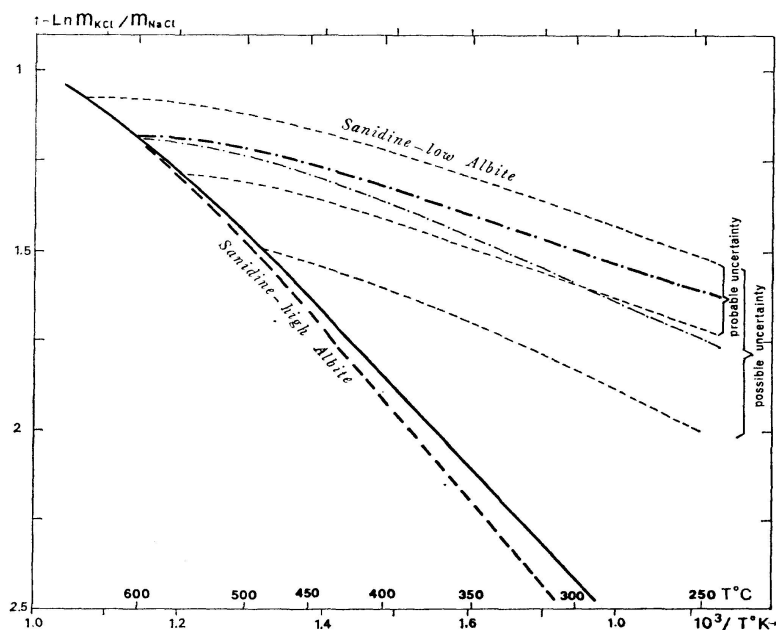
Fig. a6. The Equilibrium curves of the system Sanidine - Low Albite - KCl - NaCl aqueous solution.

Assuming the occurrence of high albite in ORVILLE's (1963) and HEMLEY's (1967) experiments (see discussion in text), we can draw the curve of equilibrium: KCl – NaCl aqueous solution – adularia – low albite, using the equation:

$$\mathrm{Ln}\left(\frac{m_{KCl}}{m_{NaCl}}\right)_L = \mathrm{Ln}\left(\frac{m_{KCl}}{m_{NaCl}}\right)_H + \frac{(\varDelta G_{Ab\ L \to H})^{P,\ T}}{RT}.$$

This curve is presented on Fig. a6 and Fig. 6.

APPENDIX III

List of the Localities

Most of the localities from which the analyzed specimens were obtained are described in the topographical mineralogy of Switzerland («Die Mineralfunde der Schweiz») by STALDER, DE QUERVAIN, NIGGLI and GRAESER, 1973. For bibliographical data refer to the above mentioned book.

In addition to the sample localities (including the coordinates of the map of Switzerland, Landeskarte der Schweiz, 1 : 25 000 and 1 : 50 000) the country rock type, the mineral paragenesis in the cleft, and the classification of the paragenesis according to PARKER (FG) (see STALDER et al., 1973) are included in the following.

Abreviations of the Mineral Names

Ab	=	Albite	Flu	=	Fluorite
Act	=	Actinolite, asbestiformeous	Gal	=	Galena
		in the Aar Massif	Hem	=	Hematite
Ad	=	Adularia	Il	=	Ilmenite
An	=	Anatase	Mon	=	Monazite
Ank	=	Ankerite	Mus	=	Muscovite
Ap	=	Apatite	Py	=	Pyrite
Br	=	Brookite	Qz	=	Quartz
Cc	=	Calcite	Rut	=	Rutile
Chl	=	Chlorite	Sid	=	Siderite
Dol	=	Dolomite	Tit	=	Titanite
Ep	=	Epidote	Tou	=	Tourmaline

Mont Blanc Massif

Trient, approximately 568.0/97.2, alt. 2000 m. Gneisses, Qz, Ad, Chl, Cc.

Le Tour, 566.9/93.7, alt. 3400 m. Granite. Qz, Ad, Chl, Cc, Ab in granite.

Charlet Straton, 566.5/89.6, alt. 3150 m. Granite. Ep, Qz, Ad, Flu, Chl, Cc, Ab in granite.

Le Tour Noir, 568.2/88.3, alt. 3300 m. Granite. Qz, Ab, Mus, Ank, Potassium Feldspar in granite.

Col des Cristaux, 567.1/85.4. Granite. Qz, Ad, Chl, Cc, Ab in granite.

Les Courtes I, 566.8/86.7, alt. 3000 m. Granite. Qz, Ad, Chl, Ab in granite.

Les Courtes II, 566.7/86.6, alt. 3300 m. Granite. Qz, Ad, Chl, Ab in granite.

Les Courtes III, 566.8/86.5, alt. 3550 m. Granite. Qz, Ad, Chl, Ab in granite.

Les Grands Montets, 562.9/88.7, alt. 3150 m. Granite. Qz, Ad, Chl, Cc, Ab in granite.

Les Rachasses, 562.7/90.2, alt. 2500 m. Gneisses. Qz, Chl, Cc.

Bochard, 560.8/88.5. Granite. Qz, Ad, Chl, Flu.

Pointe Isabelle, 567.0/85.3, alt. 3150 m. Granite. Qz, Ad, Chl, Flu, Ab in granite.

Pierre Joseph, 566.2/84.0, alt. 2850 m. Granite. Ep, Qz, Ad, Flu, Chl.

Petites Jorasses, 565.5/81.4, alt. 2900 m. Granite. Ep, Qz, Ad, Chl, Cc.

Les Periades, 562.9/80.5, alt. 3000 m. Granite. Ep, Qz, Ad, Chl, Cc, Ab in granite.

Les Mottets, 559.4/88.2, alt. 1900 m, gallery of the power station. Gneisses. Qz, Chl, Cc.

Aar Massif

Jeizel, Goppenstein, VS, approximately 625.1/133.6. Amphibolite, prehercynic basement. Qz, Ad, Cc, Ep, Act. FG 2 a.

Meiggbach, Goppenstein, VS, approximately 624.0/134.9. Amphibolite, prehercynic basement. Qz, Ad, Chl, Ep, Tit. FG 2 a.

Jägiknubel, Lötschental, VS, "at the bottom of the Jägiknubel, right side of the Langgletscher". Amphibolite, prehercynic basement. Qz, Ep, Act. FG 2 a.

Gauli, Oberhasli, BE, 659.5/163.1. Chlorite-sericite schists, prehercynic basement. Qz, Chl, Ad. FG 2 a.

Kammegg, Guttannen, BE, 667.05/168.00. Amphibolite, prehercynic basement. Qz, Ad, Chl, Ep, Act, Tit, Scheelite. FG 2 a.

Mittagfluh (Guttannen)-Trift, BE, Gallery of the hydro-electric power station Oberhasli. Chlorite-sericite schists, prehercynic basement. Qz, Cc, Chl, Ad, Py. FG 2 a.

Trift, Oberhasli, BE, approximately 671.0/171.1. Chlorite-sericite schists, prehercynic basement. Qz, Ad, Ab, Chl, Cc, An, Il. FG 2 a.

Horefelli, Voralp, UR, 682.7/169.6. Chlorite-sericite schists, prehercynic basement, near the granite contact. Qz, Ad, Chl, Flu, Tit. FG 2 a.

Vorder Ried I, Amsteg, UR, 663.25/179.65. Sericite schists, prehercynic basement. Qz (two generations, scepterquartz), Ank, Mus. FG 1 c.

Vorder Ried II, Amsteg, UR, 663.25/179.65. Amphibolite, prehercynic basement. Qz, Ab, Ad, Act, Ep. FG 1 d.

Griesserental, Maderanertal, UR. Sericite schists, prehercynic basement. Qz, Ad, Chl. FG 1 a.

Bändertal, Maderanertal, UR. Sericite schists, prehercynic basement. Qz, Ad, Chl. FG 1 a.

Staldental, Maderanertal, UR. Sericite schists, prehercynic basement. Qz, Ad, Chl, Il, FG 1 a.

Reistital, Maderanertal, UR, approximately 704.5/181.65. Sericite schists, prehercynic basement. Qz, Ad, Chl, Il. FG 1 a.

Alpgnofer Platten, Maderanertal, UR. Windgällen volcanics, ignimbrite. Qz, Chl. FG 1 a.

Ober Sand-Limmernboden, gallery of the hydro-electric power station, Linthal, GL, approximately 716.0/186.5. Tödi granite. Qz, Cc, Py. FG 1 a.

Alp Cavrein, Val Gronda, GR, 707.5/180.7. Chlorite-sericite schists. Qz, Ad, Chl, An, Br. FG 1 a.

Hinter Wasen, Fieschergletscher, VS, 654.8/149.7. Central Aar granite. Qz, Amethyst, Chl, Il, Rut. FG 4 b.

Kleines Lauteraarhorn, Grimsel, BE, approximately 654.0/158.4 Crystalline schists. Qz, Ank, Tetrahedrite, Chalcopyrite. FG 2 b.

Vorderer Zinggenstock, Grimsel, BE, 663.1/156.3. Central Aar granite. Qz, Chl, Flu, Phenakite. FG 4 a.

Juchli, Grimsel, BE, approximately 668.0/158.5. Underground discovery of 1942. Grimsel granodiorite. Qz, Chl, Cc, Flu, Py. FG 4 a.

Sommerloch I, underground, outlet gallery of the power station Oberaar, Grimsel, BE, 668.65/158.90. Grimsel granodiorite. Qz, Chl, Cc, Flu, Milarite, Ap. FG 4 a.

Sommerloch II, old historical fissure, Grimsel, BE, 668.9/159.25. Grimsel granodiorite. Qz, Chl. FG 4 a.

Unterer Kessiturm, underground, penstock of the power station Oberaar, Grimsel, BE, 668.22/157.45. Grimsel granodiorite. Qz, Mus, Cc, Sphalerite, Ank, Sid, Mon etc. FG 4 c.

Gerstengletscher, discovery of 1948, Grimsel, BE, 670.60/160.60. Grimsel granodiorite. Qz, Chl, Py. FG 4 a.

Gletschhorn, discovery of 1868, Tiefengletscher, UR, 676.3/163.65. Central Aar granite. Qz, Chl, Flu, Gal. FG 4 a.

Tiefengletscher, UR, 677.3/162.6. Central Aar granite. Qz, Chl. FG 4 a.

Göschenen I, Gotthard road tunnel N 2, safety gallery, meter 105 from the northern portal, UR. Central Aar granite. Qz, Chl, Cc. FG 4 a.

Göschenen II, Gotthard road tunnel N 2, safety gallery, meter 1925 from the northern portal, UR. Central Aar granite. Qz, Chl, Cc, Flu, Ap. FG 4 a.

Göschenen III, Gotthard road tunnel N 2, safety gallery, meter 2137 from the northern portal, UR. Central Aar granite. Qz, Cc, Ap, Chl, Tit. FG 4 a.

Fedenstock, westside, finder: X. Gnos, UR. Central Aar granite. Qz, Ab, Hem. FG 3 c.

Furggbach, Baltschiedertal, VS, 635.2/132.65. Sericite schists, prehercynic basement. Qz, Ad, Chl, Hem, Ap. FG 5 d.

Brig, fissure along the railway track of BLS, VS, 640.3/129.23. Augengneiss, prehercynic basement. Qz, Chl, Ank, Hem. FG 5 c.

Bel Grat, Belalp, VS, 639.3/139.3. Biotite-gneiss, migmatic complex of the prehercynic basement. Qz, Chl. FG 5.

Münstigergletscher, Goms, VS, 660.3/151.78. Gneiss, prehercynic basement. Qz, Ad, Chl, Hem, Ap, Chabazite. FG 5 c.

Bärfel, Oberwald, Goms, VS, 670.80/155.20. Amphibolite of the migmatite zone of St. Niklaus, prehercynic basement. Qz, Ad, Chl, Ap, Tit. FG 5 d.

Trübtensee, Grimsel, BE, 667.15/156.9. Gneis-Schiefer-Zwischenzone, prehercynic basement. Qz, Ad, Chl, Hem. FG 4 d.

Gletsch, underground, exploration gallery, VS, 670.78/157.0. Amphibolite of the migmatite zone of Gletsch, prehercynic basement. Qz, Chl, Ad, Tit, Cc, Ep. FG 5 d.

Rhonegletscher, finder: C. Simmen, 1960, Gletsch, VS. Sericite gneiss of the Gneis-Schiefer-Zwischenzone, prehercynic basement. Qz, Ad, Ap. FG 5 d.

Unter Sass, Rhonegletscher, VS, 672.1/158.6. Gneis-Schiefer-Zwischenzone, prehercynic basement. Qz, Ad, Chl, Ap, Py. FG 5 d.

Belvedere, Furka, VS, 673.1/158.63. Main migmatite zone of Gletsch, prehercynic basement. Qz, Sulfosalts, An. FG 5 d.

Grosstal, Urseren, UR, approximately 683.9/163.8. Gneiss, prehercynic basement. Qz, Ad, Chl, Ap, etc. FG 5 d.

Göschenen IV, Gotthard road tunnel N 2, safety gallery, meter 3565 from the northern portal, UR. Gneiss, prehercynic basement. Qz, Cc, Py, Chl, Laumontite. FG 5 d.

Mettlen, Andermatt, UR, 689.3/165.7. Permocarboniferous. Qz, Chl. FG 6.

Russeinbrücke, Disentis, GR, 711.45/175.60. Russeindiorite. Qz, Chl, Hem, Ep. FG 6 a.

Plattenzüg, Calanda, GR, 754.6/189.95. Spilite of the Taminser crystalline rocks. Qz, Tou, Ab, Chl. FG 15 g.

Tschengels, Calanda, GR, 751.27/190.2. Rötidolomite, Trias. Qz, Dol, Flu. FG 15 h.

Bitsch, near Brig. Penstock of the Electra Massa. Prehercynic basement, gneiss. Qz, Chl, Cc, Act. FG 5 d.

Gotthard Massif

Mooshubel, Mühlebach, VS, 654.65/139.7. Phyllite, prehercynic basement. Qz, Mus, Ank, Sid, Rut. FG 5 b.

Lamme, Fiesch, VS, approximately 654.75/139.88. Sericite schists, prehercynic basement. Qz, Ab, Cc, Mus, etc. FG 5 b.

Faulhorn, Oberwald, VS, 672.05/155.50. Sericite schists, perhercynic basement. Qz, Rut, Cc, Barite, Py. FG 5 b.

Muttengletscher, Gletsch, VS, approximately 675.0/155.8. Gurschen gneiss, prehercynic basement. Qz, Ab, Mus, Chl. FG 5 b.

Piz Prevat, Gotthard, UR, 691.0/159.2. Paragneiss, prehercynic basement. Qz, Ab, Mus, Chl, Rut, An. FG 7 b.

Ri della Fibbia, Gotthard, TI, 686.37/156.1. Fibbia granite-gneiss. Qz, Ad, Chl, Mus, Rut, Stilbite. FG 7 d.

La Fibbia, nord-east side of the mountain, Gotthard, TI. Fibbia granite-gneiss. Qz, Ad, Hem, Mus, Chl. FG 7 d.

Ri d'Albinasca, Airolo, TI, 687.1/153.4. Amphibolite, Tremolaserie s. l. Qz, Chl, Mus, Ad, Act. etc. FG 7 i.

Alpe di Fieud, Gotthard, TI, 685.85/153.5. Amphibolite, Tremolaserie s. l. Qz, Chl, Mus, Rut, Act. FG 7 i.

Grasso di Froda I, Val Canaria, gallery Unteralp-Val Canaria of the power station Ritom, meter 480 from the southern portal, TI. Biotite-gneiss, prehercynic basement. Qz, Ab, Mus, Chl, Ank, Sid, Rut, Py. FG 7 j.

Grasso di Froda II, Val Canaria, gallery Unteralp-Val Canaria of the power station Ritom, meter 490 from the southern portal, TI. Biotite-gneiss, prehercynic basement. Qz, Ab, Mus, Chl, Ank, Sid, Rut, Mon, Py. FG 7 j.

Grasso di Froda III, Val Canaria, gallery Unteralp-Val Canaria of the power station Ritom meter 1450 from the southern portal, TI. Biotite-gneiss, prehercynic basement. Qz, Ad, Ab, Mus, Chl, Cc, Py. FG 7 j.

Poncioni Negri, Val Canaria, TI, 695.4/157.8. Amphibolite, prehercynic basement. Qz, Amethyst, Ab, Mus, Sid. FG 7 i.

Alpe Stgegia I, Lukmanier, GR, 705.0/160.0. Crystallina granodiorite. Qz, Ab, Ad, Chl, Tit. FG 7 e.

Alpe Stgegia II, Lukmanier, GR, 704.72/160.66. Gneissic lense in the hercynic granite. Qz, Ab, Chl, Cc, Tou, Ap. FG 7 e.

Drual, Platta, Val Medel, GR, 708.15/168.4. Sericite schists with arsenopyrite, prehercynic basement. Qz, Ank, Gal. FG 6 f.

Piz Miez, Val Medel, GR, 706.7/159.2. Medelser granite. Qz, Ad, Chl, Mus, Rut, Tou. FG 7 e.

Val Casatscha, Val Medel, GR, 708.25/160.00. Medelsergranite. Qz, Act, Mus, Ap. FG 7 e.

Piz Garviel, Val Medel, GR, 706.9/161.0. Crystallina granodiorite. Qz, Chl. FG 7 e.

Pennines

Gh. del Cavagnöö I, Val Bavona, TI, 680.68/145.25. Psammite gneiss of the Lebendun nappe. Qz, Ad, Mus, Chl, Py, An. FG 10 e.

Gh. del Cavagnöö II, Val Bavona, TI, 680.68/145.25. Psammite gneiss of the Lebendun nappe. Qz, Ad, Ab, Chl, Mus, An, Rut, Py. FG 10 e.

Gh. del Cavagnöö III, Val Bavona, TI, 680.76/145.30. Psammite gneiss of the Lebendun nappe. Qz, Ad, Ab, Cc, Mus, An, Py, Ank. FG 10 e.

Gh. del Cavagnöö IV, Val Bavona, TI, 680.62/145.15. Psammite gneiss of the Lebendun nappe. Qz. FG 10 j.

Cavagnöö, supply gallery of the power station Maggia, close to the entrance of the gallery. Gneiss. Qz, Ad, Mus, Chl, Rut, Ank, Py. FG 10 f.

Poncione di Braga, Alpe Masnaro, Val di Peccia, TI. Gneiss. Qz, Chl, Mus, Hem. FG 10 e.

Lago Bianco, Val Bavona, TI, approximately 682.3/145.3. Gneiss. Qz, Mus, Cc, Ank. FG 10 f.

Pizzo dell'Arzo, Val Bavona, TI, 680.65/144.55. Gneiss of the Lebendun nappe. Qz, Ad, Mus, Rut. FG 10 e.

Fusio, Val Lavizzara, TI, 694.0/145.0. Gneiss. Qz, Ad, Chl, An. FG 10 e.

Pizzo Madone I, Val Torta, TI, 685.6/149.3. Bündner schists. Qz, Mus, Rut, Pyrrhotite. FG 10 d.

Pizzo Madone II, Val Torta, TI, 685.25/149.13. Bündner schists. Qz, Chl, Tou. FG 10 d.

Alpe di Ravina, Airolo, TI. Bündner schists. Qz, Mus, Py. FG 10 d.

Pizzo Gararesc, Val Cassinello, Val Bedretto, TI. Gneiss. Qz, Ab, Ad, Mus, Cc. FG 10 e.

Laghetti, Naret, Val Sambuco, TI, 688.4/147.12. Granite gneiss. Qz, Chl. FG 10 e.

Naret, Val Sambuco, TI. Amphibolite. Qz, Ab, Chl, Tit, Il. FG 10 h.

Val di Chironico, Val Leventina, TI, 703.0/140.5. Gneiss. Qz, Ad, Tit. FG 10 h.

Pizzo Barone, Val di Chironico, Val Leventina, TI, 700.5/140.5. Biotite gneiss. Qz. FG 10 h.

Iragna, Riviera, TI, 717.9/131.0. Granite gneiss of the Leventina. Qz, Ad, Chl, Ep, Tit. FG 10 g.

Aquarossa, Val Blenio, TI, 715.5/145.4. Gneiss. Qz, Ad, Ab, Mus, Cc, Tou, Rut, Sid etc. FG 10 e.

Prugiasco, Val Blenio, TI, 714.72/146.17. Granite gneiss. Qz, Chl, Mus, Ab, Rut, Ap, Ank, Tou. FG 10 f.

Arvigo, Val Calanca, GR, 729.0/128.9. Granite gneiss. Qz, Ad, Chl, Mus, Cc, Ep, Tit, Zeolites etc. FG 10 g.

Camperio, Olivone, TI (fissure nr 70 of A. Wagner), 711.70/153.65. Bündner schists, calciferous garnet schists of the lower Stgir serie. Qz, Ank, Cc, Chl, Mus, Tou, Rut, Scapolite etc. FG 10 d.

Campo Blenio, Val Blenio, TI, 714.8/156.2. Bündner schists. Qz, Ab, Chl, Mus, different iron ores. FG 10 d.

Paltano, Val Bedretto, TI, 677.94/147.06. Bündner schists. Qz, FG 10 i.

Piz Stgir, Greina, GR, 721.54/165.8. Bündner schists. Qz, Cc. FG 8 h.

Val Largia, Lumnezia, GR, 725.98/169.58. Bündner schists. Qz, Cc. FG 8 h.

Stockchnubel, Gornergletscher, VS, 630.2/92.2. Mica schists from the Stockchnubel-Schuppenzone. Qz, Ad, Cc, Chl, Ep, Laumontite. FG 12 c.

Fluh, St. Niklaus, Mattertal, VS, approximately 628.2/112.8. Trias quartzite. Qz, Ab, Mus. FG 13 a.

Simplontunnel I, meter 5342-49 from the northern portal. Berisalschists. Qz, Chl, Mus, Ank. FG 11 f.

Simplontunnel II, meter 5528-32 from the northern portal. Berisalschists. Qz, Amethyst, Chl. FG 11 f.

Simplontunnel III, meter 5730-38 from the northern portal. Berisalschists. Qz, Chl, Cc, Hem. FG 11 f.

Simplontunnel IV, meter 6462-68 from the northern portal. Berisalschists. Qz, Chl, Mus, Ad, Ank. FG 11 f.

Gibelmatten, Längtal, Binntal, VS. Gneiss of the Monte Leone nappe. Qz. FG 11 d.

Lengenbach, Feld, Binntal, VS, 660.16/135.14. Sugar-grained dolomite. Qz, Hyalophane, Mus, Sulphides, Sulfosalts etc. FG 11 b.

Gischihorn, Kriegalptal, Binntal, VS, 659.65/130.05. Gneiss of the Monte Leone nappe. Qz, Tou, Hem, Rut, Mus, Chernovite. FG 11 d.

Albrunhorn, Binntal, VS, 664.5/135.4. Gneiss of the Monte Leone nappe. Qz, Ep. FG 11 d.

Herkumme, Blinnental, VS. Bündner schists. Qz, Cc, Rut, Ank, Sphalerite. FG 11 a.

REFERENCES

ARNOLD, A. (1972): Rb-Sr-Untersuchungen an einigen alpinen Zerrklüften des Cristallina-Granodiorites im östlichen Gotthardmassiv. Schweiz. Min. Petr. Mitt. 52/3, p. 537–551.

BURNHAM, C. W., HOLLOWAY, J. R., DAVIS, N. F. (1970): Thermodynamic properties of water to 1000° C and 10000 bars. Geol. Soc. of Amer., Special paper 132.

CLARK, S. P. JR. and JÄGER, E. (1969): Denudation rate in the Alps from geochronologic and heat flow data. Am. J. Sci., 267, p. 1143–1160.

McCONNELL, J. D. C. and McKIE, D. (1960): The kinetics of the ordering process in triclinic $NaAlSi_3O_8$. Mineral. Mag. 32, p. 436–454.

DEICHA, G. (1949): Thermométrie comparée dans quelques minéraux alpins du massif du Mont-Blanc. Bull. Soc. fr. de Minér., 72, p. 355–358.

— (1955): Les lacunes des cristaux et leurs inclusions fluides. Masson et Cie., Paris, 126 p.

DENBIGH, K. (1968): The Principles of Chemical Equilibrium, 2nd edition, Cambridge.

FOURNIER, R. O and TRUESDELL, A. H. (1973): An empirical Na-K-Ca geothermometer for natural waters. Geoch. Cosm. Acta, 37, p. 1255–1275.

GAMMON, J. B., BORCSIK, M. and Holland, H. D. (1967): The composition of an aqueous phase in equilibrium with melts of granitic composition (abstr.). Trans. Amer. Geophys. Union, 48, 245.

GRIGORIEV, D. P. (1960): The origin of quartz as a fissure mineral of the Alpine type with special reference to occurences in the U.S.S.R. Cursillos y Conferencias del Instituto "Lucas Mallada" VII, Madrid, p. 63–76.

GUSTAFSSON, L. (1960): Determination of ultramicro amounts of sulphate as methylene blue. I the colour reaction. II the reduction. Talanta vol. 4, p. 227–243.

HELGESON, H. C. (1967): Solution chemistry and metamorphism, in Abelson, Researches in Geochemistry, 2, John Wiley and Sons.

— (1968): Evaluation of irreversible reactions in geochemical processes involving minerals and aqueous solutions. I: thermodynamic relations. Geoch. Cosm. Acta, 32, p. 853–877.

HELGESON, H. C., GARRELS, R. M. and MACKENZIE, F. T. (1969): Evaluation of geochemical processes involving minerals and aqueous solutions. II: applications. Geoch. Cosm. Acta, 33, p. 455–481.

HEMLEY, J. J. (1967): Aqueous Na/K ratios in the systems K_2O-Na_2O-Al_2O_3-SiO_2-H_2O (abstract). Programm, Ann. Meeting, Geol. Soc. Amer., p. 94–95.

HOLLAND, H. D. (1967): Gangue minerals in hydrothermal deposits. In BARNES, H. L.: Geochemistry of hydrothermal ore deposits. Holt, Rinehart and Winston, Inc., p. 382–436.

HOLM, J. L. and KLEPPA, O. J. (1968): Thermodynamics of the disordering process in albite. Amer. Min. 53, 123–133.

HOVIS, G. L., WALDBAUM, D. R. and THOMPSON, J. B. JR. (1970): Calorimetric studies of Al-Si ordering and Na-K mixing in monoclinic alkali feldspars. Geol. Soc. Amer. Abstracts with Programs, 2, 582.

JÄGER, E., NIGGLI, E. and WENK, E. (1967): Rb-Sr-Altersbestimmungen an Glimmern der Zentralalpen. Beitr. geol. Karte Schweiz, NF 134.

IIYAMA, T. (1970): Influence de la pression sur la composition de la solution hydrothermale sodi-potassique de divers sels en équilibre avec les feldspaths perthitiques à 600° C. Observation expérimentale. C.R. Acad. Sci. Paris, t. 271, p. 1925–1927.

JOHNSON, C. M. and NISHITA, H. (1952): Micro-estimation of sulfur in plant materials, Soils, and irrigation waters. Anal. Chem., V. 24, p. 736–742.

KOENIGSBERGER, J. and MÜLLER, W. J. (1906): Über die Flüssigkeitseinschlüsse im Quarz alpiner Mineralklüfte. Cbl. Mineral., p. 72–77.

KOENIGSBERGER, J. (1917–1919): Über alpine Minerallagerstätten I.–III. Teil. Abh. bayer. Akad. Wiss., math.-phys. Kl. 28, Abh. 10–12.

LACROIX, A. (1962–1964): Minéralogie de la France et de ses anciens territoires d'outremer. Tome premier – tome sixième, A. Blanchard, Paris.

LANDOLT-BÖRNSTEIN (1960): Eigenschaften der Materie in ihren Aggregatzuständen. 2. Band, 2. Teil, Bandteil a. Springer-Verlag.

LARSEN, S. D. (1956): Phase studies of the two component carbon dioxide-water system involving the carbon dioxide hydrate. Univ. Microfilms No. 15235, Ann Arbor, Mich. (Diss. Abstr.) 16, 248.

LEMMLEIN, G. G. and KLEVTSOV, P. V. (1961): Relations among the principal thermodynamic parameters in a part of the system H_2O-$NaCl$. Geochemistry, Vol. 2, p. 148 to 158.

LEROY, J. (1971): Les épisyénites non minéralisées dans le massif de granite à deux micas de Saint-Sylvestre (Limousin-France). Thèse, Université de Nancy I, 87 p.

LEUTWEIN, F., POTY, B., SONET, J. and Zimmermann, J.-L. (1970): Age des cavités à cristaux du granite du Mont Blanc. C.R. Acad. Sc. Paris, 277, p. 156–158.

MARTIN, R. F. (1969): The hydrothermal synthesis of low albite. Contrib. Min. Petrology, 23, 323–339.

MULLIS, J., POTY, B. and LEROY, J. (1973): Nouvelles observations sur les inclusions à méthane des quartz du Val d'Illiez, Valais (Suisse). C.R. Acad. Sc. Paris, 277, p. 813 à 816.

NIGGLI, P., KOENIGSBERGER, J., PARKER, R. L. (1940): Die Mineralien der Schweizeralpen, Band I und II, Wepf & Co., Basel, 661 p.

ORVILLE, P. M. (1963): Alkali ion exchange between vapor and feldspar phases. Am. J. of Science, 261, p. 201–237.

PARKER, R. L. (1954): Die Mineralfunde der Schweizer Alpen. Wepf & Co., Basel, 311 p.

POTY, B. (1969): La croissance des cristaux de quartz dans les filons sur l'exemple du filon de La Gardette (Bourg d'Oisans) et des filons du massif du Mont-Blanc. Thèse, Université de Nancy, 161 p.

POTY, B. and STALDER, H. A. (1970): Kryometrische Bestimmungen der Salz- und Gasgehalte eingeschlossener Lösungen in Quarzkristallen aus Zerrklüften der Schweizer Alpen. Schweiz. Min. Petr. Mitt. 50/1, p. 141–154.

PURDY, J. W. and STALDER, H. A. (1973): K-Ar Ages of Fissure Minerals from the Swiss Alps. Schweiz. Min. Petr. Mitt. 53/1, p. 79–98.

QUIST, A. S. and MARSHALL, W. L. (1968): Electrical conductances of aqueous sodium chloride solutions from 0 to 800° C and at pressures to 4000 bars. J. Phys. Chem., 72, p. 684–703.

RITZERT VON, G. and FRANCK, E. U. (1968): Elektrische Leitfähigkeit wässriger Lösungen bei hohen Temperaturen und Drucken. I Ber. Bunsengesellschaft. physikal. Chemie, 72, 7, p. 798–808.

ROBIE, R. A. and WALDBAUM, D. R. (1968): Thermodynamic properties of Minerals and related substances. ... Geol. Survey Bull. 1259.

ROBINSON, R. A. (1961): Activity coefficients of sodium chloride and potassium chloride in mixed aqueous solutions at 25° C. J. Phys. Chem., 65, p. 662–667.

RODEBUSH (1918): J. Amer. chem. Soc., 40, 1204.

ROEDDER, E. (1962): Studies of fluid inclusions I: Low temperature application of a dual-purpose freezing and heating stage. Economic Geol. 57, p. 1045–1061.

— (1963): Studies of fluid inclusions II: Freezing data and their interpretation. Economic Geol. 58/2, p. 167–211.

ROEDDER, E., INGRAM, B. and HALL, W. E. (1963): Studies of fluid inclusions III: Extraction and quantitative analysis of inclusions in the milligram range. Economic Geol. 58, p. 353–374.

ROEDDER, E. (1967): Fluid inclusions as samples of ore fluids. In Barnes, H. L.: Geochemistry of hydrothermal ore deposits. Holt, Rinehart and Winston, Inc., p. 515–574.

— (1970): Application of an Improved Crushing Microscope Stage to Studies of the Gases in Fluid Inclusions. Schweiz. Min. Petr. Mitt. 50/1, p. 41–58.

SCATCHARD and PRENTISS (1933): J. Amer. Chem. Soc. 55, 4355.

STALDER, H. A. (1964): Petrographische und mineralogische Untersuchungen im Grimselgebiet (Mittleres Aarmassiv). Schweiz. Min. Petr. Mitt. 44/1, p. 187–398.

— (1967): Abhängigkeit einiger alpiner Mineralgesellschaften von der Zusammensetzung des hydrothermalen Lösungsmittels. Schweiz. Min. Petr. Mitt. 47/2, p. 1124–1131.

STALDER, H. A. and TOURAY, J. C. (1970): Fensterquarze mit Methan-Einschlüssen aus dem westlichen Teil der schweizerischen Kalkalpen. Schweiz. Min. Petr. Mitt. 50/1, p. 109–130.

STALDER, H. A., DE QUERVAIN, F., NIGGLI, E., GRAESER, S. (1973): Die Mineralfunde der Schweiz, 433 p., Wepf & Co., Basel.

STERN, J. H. and ANDERSON, C. W. (1964): Thermodynamic properties of aqueous solutions mixed electrolytes. J. Phys. Chem., 68, p. 2528–2533.

THOMPSON, J. B. JR. (1967): Thermodynamic properties of simple solutions, in Abelson, Researches in Geochemistry, 2, John Wiley & Sons.

THOMPSON, J. B. JR. and WALDBAUM, D. R. (1968): Mixing properties of sanidine crystalline solutions; I. Amer. Mineral., 53, p. 1965–1999.

TOURAY, J. C. (1968): Recherches géochimiques sur les inclusions à CO_2 liquide. Bull. Soc. franç. Mineral. Crist., 91, p. 367–382.

TOURET, J. (1971): Le facies granulite en Norvège meridionale, I and II. Lithos 4, p. 239 to 249 and 423–436.

WALDBAUM, D. R. and THOMPSON, JR. (1969): Mixing properties of sanidine crystalline solution: IV. Amer. Mineral., 54, p. 1274–1298.

WALDBAUM, D. R. and ROBIE, R. A. (1971): Calorimetric investigations of Na-K mixing and polymorphism in the alkali feldspars. Zeitschrift für Kristallographie, 134, p. 381–420.

WELLMAN, T. R. (1970): Fugacities and activity coefficients of NaCl in $NaCl-H_2O$ fluids at elevated temperatures and pressures. Amer. J. of Science, 269, p. 402–413.

WIEBE, R. and GADDY, V. L. (1940): The solubility of carbon dioxide in water at various temperatures from 12° to 40° and at pressures to 500 atmospheres – Critical phenomena. Amer. Chem. Soc. J., 62, p. 815–817.

YPMA, P. J. M. (1963): Rejuvenation of ore deposits as examplified by the Belldonne metalliferous province. Proefschrift, Leiden, 212 p.

ZIMMERMANN, J. L. and POTY, B. (1970): Etude par spectrométrie de masse de la composition des fluides dans les cavités alpines du massif du Mont Blanc. Schweiz. Min. Petr. Mitt. 50/1, p. 99–108.

PLATE I

Approximate Composition of the Fluid Inclusions in
Alpine Quartz Crystals. Central Part of the Swiss Alps
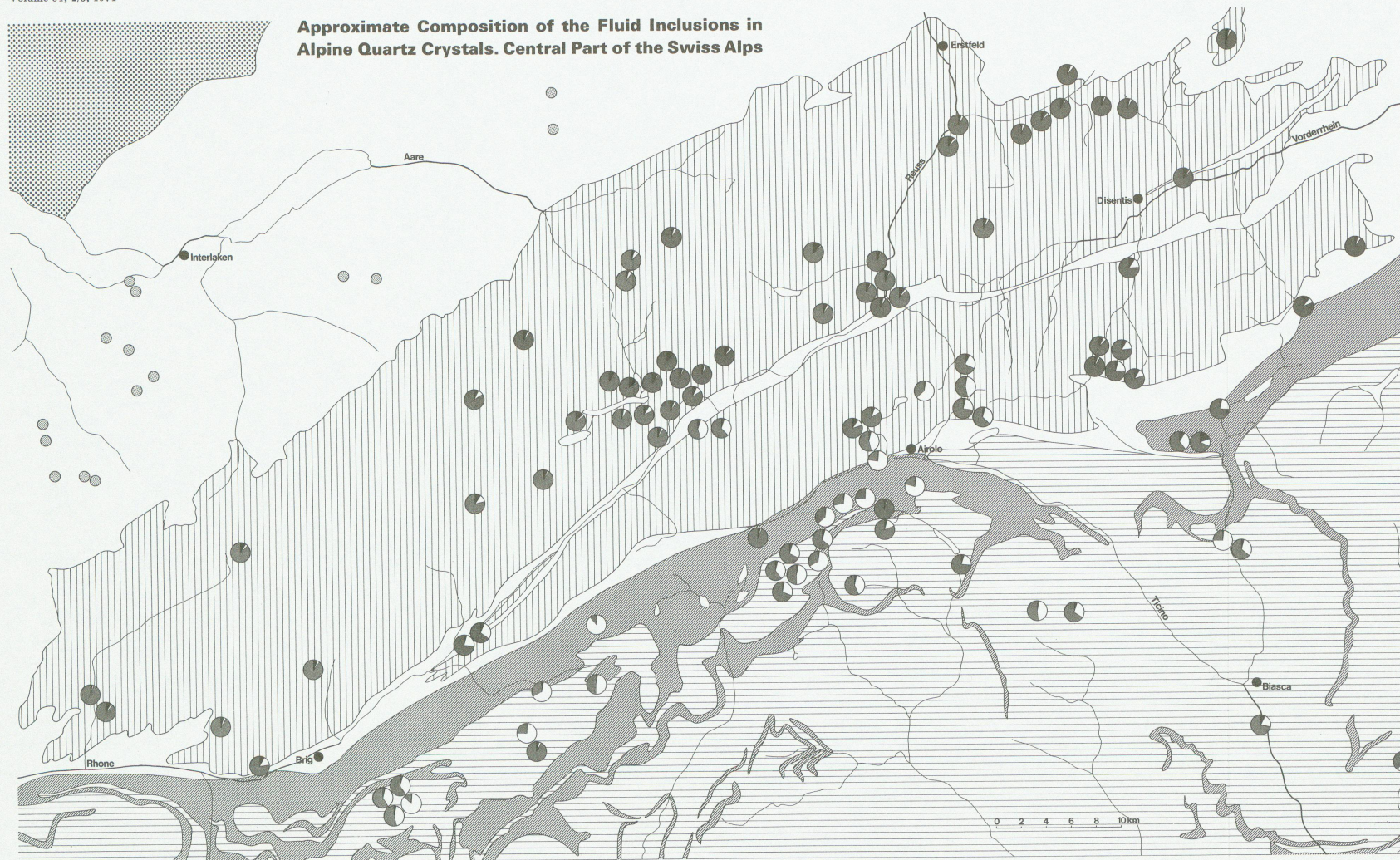
Geology

Molasse Basin. Younger Tertiary Sediments

Helvetic and Ultrahelvetic Zone (incl. other
tectonic units in the NW): Permian to Tertiary
Sediments

Pennine Mesozoic Rocks

Other Pennine Rocks

Aar- and Gotthard Massif (incl. Tavetscher
Massif): Pre-Triassic Crystalline Rocks

Fluid Inclusions in the Fissure Quartz Crystals

Equivalents NaCl in Weight Percents

CO_2 in Weight Percents

H_2O in Weight Percents

Quartz Occurences with more or less pure
Methane Inclusions besides Inclusions with an
Aqueous Solution (after Stalder and Touray,
1970)

Interlaken

Aare

Reuss

Erstfeld

Disentis

Vorderrhein

Airolo

Ticino

Biasca

Rhone

Brig

0 2 4 6 8 10 km